AN EXAMINATION OF THE TWO KINETIC REGIMES OF THE NITRIC OXIDE-CARBON GASIFICATION REACTION

E.M. Suuberg, H. Teng, and I. Aarna
Division of Engineering, Brown University,
Providence, RI 02912

Keywords: Nitric Oxide, Carbon, Gasification

INTRODUCTION

The reaction of NO with carbon has been shown by many workers to involve two distinct rate regimes, at temperatures of practical interest [1,2]. Based upon our earlier results, we suggested that the two regimes most likely involve rate control by site creation in the low temperature regime and dissociative chemisorption in the high temperature regime. Further experiments and analysis will be presented here in support of these hypotheses.

The mechanism of the NO-carbon reaction has been suggested to involve the following steps [2]:

$$2\,C + NO \rightarrow C(O) + C(N) \quad (R1)$$

$$C + C(O) + NO \rightarrow C(O_2) + C(N) \quad (R2)$$

$$2\,C + 2\,NO \leftrightarrow 2\,C(NO) \quad (R3)$$

$$C^* + C(O) + NO \rightarrow CO_2 + C(N) + xC^* + x'C \quad (R4)$$

$$C^* + NO \rightarrow CO + C(N) + yC^* + y'C \quad (R5)$$

$$C(O) \rightarrow CO + a\,C^* + a'C \quad (R6)$$

$$C(O_2) \rightarrow CO_2 + b\,C^* + b'C \quad (R7)$$

$$2\,C(N) \rightarrow N_2 + d\,C^* + d'C \quad (R8)$$

The reaction (R3) is only important at quite low temperatures (< 473K) [4]. The reactions (R1) and (R2) are dissociative chemisorption on non-rapid turnover sites [2]. The reactions involving C* are the rapid turnover site reactions, that yield both CO via (R5) and CO_2 via (R4). The reaction (R2) allows for some small amounts of stable CO_2-forming complex on the surface. The reactions (R6), (R7) and (R8) reflect formation of empty rapid turnover sites C*, as well as non-rapid turnover sites, C. The exact nature of the C* sites and C sites, and what makes them different, is unclear. Thus the stoichiometry of their formation is also unclear. The reactions (R6)-(R8) are governed by distributions of activation energies, and (R6) and (R7) make a large contribution to the overall rate at low temperatures [1,2]. In fact, the rapid turnover processes (R4) and (R5) are probably governed by the same continuum of activation energies as are (R7) and (R6), respectively, except that at any given temperature, certain sites are effectively immediately desorbed upon formation.

The low desorption activation energy surface species, for which the rate of desorption is quite fast compared to the rate of their formation by dissociative chemisorption of NO, give rise to surface sites that are normally "empty" (the C* sites). Again, it is probably impossible at the present time to define a particular reaction pathway for a particular type of site. The concept of a rapid turnover site is largely a bookkeeping construct. Without direct evidence to support the view that there exists a particular carbon structure C* which will, upon oxidation, immediately desorb as part of CO or CO_2, it is more prudent to adopt a more flexible view of what C* might represent. It may well be the case that chemisorption on one surface site will tend to destabilize another, neighboring oxide structure. This view is supported by the recent insightful isotope labeling experiments of Orikasa et al. [5] , which suggested that the rate of (R6) might be enhanced by processes involving participation by NO itself (though a thermal artifact was seemingly not ruled out). Kinetically, the transient behavior observed by these workers at 873 K appeared consistent with a rapid turnover process such as (R5), and the isotopic composition showed that some of the oxygen came from oxide on the surface [5]. Thus it might be necessary to define C* more broadly, so as to include not only a carbon structure that is able to be oxidized, but also possibly neighboring carbon oxide sites. A similar suggestion has been advanced by Tomita and coworkers [6,7]. This represents a considerable step in the direction of increasing complexity of models of the oxidation process.

Here, we consider some new experimental results that help to shed further light on models of NO reaction with carbon. In particular, we explore further the role of surface oxides in determining the rate of the reaction processes in both the high and low temperature regimes. These two regimes have been discussed elsewhere [1,2], and typical two-temperature regime behavior is seen in Figure 1, which will be discussed below.

EXPERIMENTAL

Two different thermogravimetric analyzer (TGA) reactor systems have been used in this study; one from TA Instruments and the other from Cahn Instruments. The TA Instruments TGA has a somewhat smaller enclosed gas volume than does the Cahn system, thus, the experiments in the TA Instruments TGA were performed with a continuous gas flow through the TGA to ensure that depletion of NO was not significant. Apart from this small difference, the TGA work was

performed as earlier described[1,2], and the results indicate no significant differences attributable to the particular TGA system used. As is usual in our TGA work, experiments were performed at quite high NO partial pressures, ranging from about 1 to 10 kPa of NO partial pressure. The reaction has been shown to be first order in NO over a very wide range of pressures [3], and the rates from this range of pressures can be extrapolated with confidence to lower partial pressures.

Some experiments were performed in a packed bed reactor system. This reactor consisted of a 4 mm ID quartz tube packed with around 100-200 mg of char, giving a bed length of order 10-30 mm. The NO concentrations examined in this system were much lower than those in the TGA system, and ranged from about 1 to 20 Pa.

One material selected for study is a char derived from phenol-formaldehyde resin. It has been described before [1,2]. This material has a relatively low impurity content. The material has been heat treated at 1323 K for two hours prior to any experiments. A second material is a char derived from Wyodak coal char. This char was derived from a sample of the Argonne Premium Coal Sample Program [8]. Details of its pyrolysis will be discussed below.

The chars were also subjected to "surface cleaning" in some cases. This procedure involves exposure of the char to high-pressure flowing helium at either 1223 or 1273 K for one to two hours. This results in removal of most, though not all, of the desorbable oxides from the surface. The amount of surface oxides that remains after surface cleaning is difficult to establish, quantitatively. The rate of oxide desorption at the end of the the surface cleaning process is generally quite low, when the process is stopped.

Results and Discussion

Factors Affecting the Active Site Concentration

Typical results of the experiments on the resin char, at an NO partial pressure of 2 kPa, are shown in Figure 1. The results are shown as first order rate constants for the destruction of NO on the carbon surface. The data show the previously discussed two-temperature-regime behavior. Two different types of experiments are shown and both show the two-regime behavior. One set was performed as previously described [1,2]. Samples were subjected to a sequence of different temperatures, under a constant NO partial pressure. Different temperatures were explored by simply changing the temperature of the reactor. To hasten achievement of pseudo-steady state behavior, these experiments were performed by starting the experimental sequence at high temperatures. No attempt was made to clean the surface of oxides between each temperature step. These experiments will be referred to as those involving an "uncleaned" surface. These experiments gave relatively constant rates of mass loss (the main experimentally measured quantity) over timescales of tens of minutes, and these are what are reported in Figure 1. The approach to apparent steady state was generally faster, the higher the temperature.

A second set of experiments was performed with an identical material, but with a different experimental procedure. The difference had to do with how the surface was prepared for an experiment. Rather than permitting the oxides to remain on the surface throughout the experimental sequence, in this case, each time the temperature was changed, the oxides were desorbed (to a significant extent) by heating the sample at 1223 K for two hours. These experiments are described as involving a "cleaned" surface. This somewhat more tedious experimental procedure had been earlier followed in experiments designed to determine the true order of reaction [1]. In that case, it had been observed that leaving the oxides on the surface gave an apparent non-unity order with respect to NO, particularly in the high temperature regime. This was because the timescale for the oxide population to adjust itself to a different pressure was sufficiently long (many hours) that it was easy to miss this fact in experiments in which the appearance of linear mass loss with time was used to judge approach to pseudo-steady state. In the experiments reported here, the rates were again taken to be those at apparent pseudo-steady state, consistent with how the rates were determined for the uncleaned samples.

Comparison of the results of experiments with cleaned and uncleaned samples shows that in the low temperature regime (below about 1000 K), the rate of the reaction is clearly higher with the surface cleaned samples. In the high temperature regime, no significant differences have been noted between cleaned and uncleaned samples in these, or any other, experiments. Thus there is suggestion that the existence of oxides on the surface can retard the apparent rate of the gasification under certain circumstances, commensurate with the above model in which the C* is viewed as depending upon free sites for rapid turnover [2]. It should be noted that this result is not a consequence of "thermal annealing" [9], in that the more highly heat treated carbon (that with the surface cleaned after each cycle) is more reactive than the sample for which this is not done. These results at first appear to be in direct contradiction to those reported by Suzuki et al. [7], in which oxidation of a carbon surface enhanced the rate of reaction with NO. It is possible that the discrepancy arises from the different degree or nature of oxidation (or surface cleaning) in the two studies. Suzuki et al. used O_2 to oxidize the surface, and the complexes created by oxygen may be different than those created by NO. We have seen evidence of this difference in TPD studies. Further, it has been noted by Tian [10] that addition of H_2 to an NO containing mixture increases the rate of NO destruction. Tian's experiments were conducted at 1073 K, and appeared to be in what we term the high temperature regime, so it is unclear that they can be compared directly with the present results. Nevertheless, they are clearly suggestive of a role of oxide removal in rate

enhancement.

Similar types of experiments have been performed at significantly lower NO partial pressures in the packed bed reactor. The effect of surface cleaning is barely visible (and of course the overall reaction rates are much lower). This means that the effect of surface oxide population is associated with the partial pressure of NO. The pseudo-steady population of surface oxides increases with increase in NO pressure, though this dependence is very weak at high NO pressures [1], possibly indicating surface saturation. There is, however, evidence that the reaction shows a higher order dependence upon NO pressures when NO pressures become low (of order 1 Pa). This would be expected, as reactions such as (R2) and (R4) become "starved" for surface oxides. The concentration of surface oxides would be expected to become more sensitive to the NO pressure, as the pressure of NO is decreased (as may be reasoned from a simple Langmuir-type adsorption model).

We have also studied the effect of differences in active site density in another way, as shown in Figure 2. This figure illustrates the effect of heat treatment on Wyodak coal char. One char was prepared by heating at 1273 K for a total of four hours, while the other was heated up to a temperature of 1273 K, at a rate of 30 K/min, and then immediately cooled. The results of Figure 2 show one facet consistent with what was seen in Figure 1 - the effects of heat treatment are most notable in the low temperature regime, and largely disappear in the high temperature regime. Here, however, the less highly heat-treated char, which presumably contains more active sites to begin with, was not surface cleaned during the experimental sequence (in fact, each point was obtained with a "fresh" sample). The more highly heat treated char was surface cleaned. The less highly heat treated material would have had more active sites to begin with, and would have retained these, but for filling with oxides. The change in the population of sites with time was not explored. Thus the conclusion from these experiments is that thermal annealing effects can and do play the usual sort of role in influencing reactivity, but the effects are different in the two temperature regimes. It may be further concluded, by comparing with Figure 1, that surface cleaning may affect the extent of annealing, but by the time a sample has already been heat-treated for several hours at 1273 K, the annealing effects become less important than the site-blockage effects.

There are two general conclusions which may be drawn based upon these results. The first is that examination of the rates and dynamics of the NO-carbon reaction must always establish in which temperature regime the processes of interest are occurring. There is no possibility of deriving "general" conclusions concerning mechanism without careful consideration of this point. There is ample evidence of very long timescale dynamics associated with rearrangement of surface oxides, which, in turn, can significantly affect the observed rates. The effects of NO partial pressure must also be taken into account. The second general conclusion is that the rates in the low temperature regime appear to be generally more sensitive to any factors that affect active site populations than are rates in the high temperature regime. It is already clear that the process of NO destruction (or gasification) is somehow different at the higher temperatures. It is possible that a different set of active sites begins to dominate the rate because a different reaction pathway becomes favorable, or it might be that as a result of an increase in available active sites, a second step in a reaction pathway becomes limiting. We have earlier suggested this latter possibility [2].

The Kinetic Role of The Rapid Turnover Active Site Population

The relative roles of the desorption processes such as (R6) compared to the rapid turnover processes such as (R5) has been earlier examined, using the resin char [2]. The rate of carbon gasification is given by the sum of contributions from the desorption processes and the processes such as (R5): $r=r_a+r_d$, where r_d corresponds to (R6) and r_a to (R5). The focus on CO-yielding reactions is chosen for simplicity; the analysis may be extended to include CO_2 as a product as well, at the expense of greater complexity. The data on the overall rate, r, and the desorption rate in the absence of NO, r_d, have been given elsewhere [2]. Noting that $r_a = k_a[C^*]P_{NO}$ and $r_d = k_d[C(O)]$, then it can be seen that:

$$d[\ln (r_a/r_d)]/d[1/T] = - (E_a-E_d)/R + d \ln [C_{tot}/C^* -1] /d [1/T]$$

where C_{tot} is the total number of sites in either the form C* or C(O). Working at the limit $C^*/C_{tot}<<1$, i.e., most sites are oxide-filled, allows the above result to be approximated as:

$$d[\ln (r_a/r_d)]/d[1/T] = - (E_a-E_d)/R - d \ln [C^*] /d [1/T]$$

The left hand side of the above equation is shown in Figure 3, yielding a slope of - 3969 K. The value of the last term on the right hand side is evaluated from experiments in which the free sites are filled at a temperature below gasification (see ref. 2). The result is also seen in Fig. 3, and define a slope with $(1/T)$ of -7100 K. The rate of desorption of oxides from the surface was tracked in TGA experiments in which the mass loss rate was followed after removal of NO [1,2]. These data are also represented in Figure 3, yielding an apparent E_d = 89 kJ/mol. Combining the above values yields E_a = 181 kJ/mol, in good agreement with the experimentally determined value for the high temperature range (e.g., Figure 1).

It is noteworthy that the above calculation spanned both the high and low temperature ranges, using data from each. The results of the kinetic calculation are very much in concert with the earlier conclusion, based upon product analyses, that both (R5) and (R6) type reactions occur in both temperature regimes [2]. The fact that reactions of type (R5) appear to play a significant kinetic role

in the low temperature regime cannot be overlooked, even though their inherent activation energy is seen only in the high temperature regime. It is the competition between these reactions, at any particular temperature, that determines the apparent kinetic constants. We have also observed that the shift from low-temperature to high-temperature regimes occurs at widely varying temperatures in different carbons, so it is not possible to make a general statement about which processes may be neglected at what temperatures.

Based upon this analysis, and our earlier results, it is clear that there exists a population of sites that is "empty" (available for reaction) under all reactive conditions, and at which rapid turnover processes occur with an activation energy characteristic of the high temperature regime. The population of such sites appears to increase with increasing temperature. The numbers of such sites depend upon how the sample was prepared (how highly heat treated it was) and how heavily the surface is oxidized. As the temperature of the surface is raised, the population of empty sites increases (due to desorption of oxides) to such an extent that the rate begins to show the thermal dependence of the decomposition of NO on the sites. This defines the high temperature regime. At lower temperatures, the temperature dependence of the overall rate reflects the temperature dependence of desorption processes, since these not only contribute product via reactions such as (R6), but also free up sites for reactions such as (R5). This model will be formalized in a forthcoming paper.

ACKNOWLEDGEMENT

We gratefully acknowledge the financial support provided by the USDOE under grant DE-FG22-94PC94218.

REFERENCES

1.Suuberg, E.; Teng H.; Calo, J. *23rd Symp. (Int.) on Combustion*, The Comb. Inst., Pittsburgh, 1990; p 1199.
2. Teng, H.; Suuberg, E.M.; Calo, J.M. *Energy and Fuels*, **1992**, *6* , 398.
3. Aarna, I.; Suuberg, E.M., paper presented at this meeting.
4. Teng, H.; Suuberg, E.M. *J. Phys. Chem.*, **1993**, *97*, 478.
5. Orikasa, H.; Suzuki, T.; Kyotani, T.; Tomita, A.; Martin, R., *Proc. Carbon '95*, p 626, American Carbon Society, 1995.
6. Yamashita, H.; Tomita, A.; Yamada, H.; Kyotani, T.; Radovic, L.R., *Energy Fuels*, **1993**, *7*, 85.
7. Suzuki, T.; Kyotani, T.; Tomita, A., *I&EC Res.*, **1994**, *33*, 2840.
8. Vorres, K. *Energy and Fuels*, **1990**, *4*, 420.
9. Suuberg, E.M. in *Fundamental Issues in Control of Carbon Gasification Reactivity* (J. Lahaye and P. Ehrburger, Eds.), p. 269, Kluwer, Boston, 1991.
10. Tian, Y., Doctoral Dissertation, Chemistry, University of Essen, Germany, 1993.

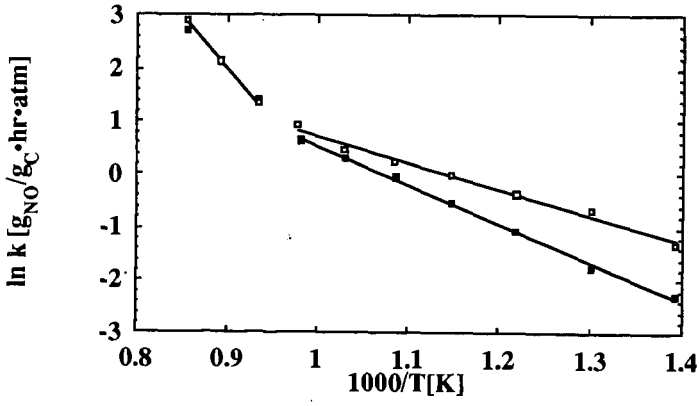

Figure 1. A comparison of the rate constant for NO reduction by resin char with cleaned surface (open squares) and uncleaned surface (closed squares). The NO pressure was 2 kPa.

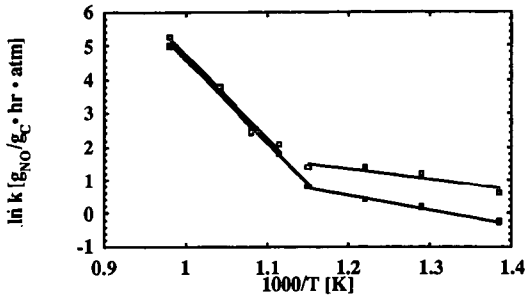

Figure 2. The effect of heat treatment upon the reactivity of Wyodak char. The open points are for a sample heated to 1273 K at 30 K/min, and the closed points are for a sample heated for four hours at 1273 K (see text). The NO partial pressure was 10 Pa.

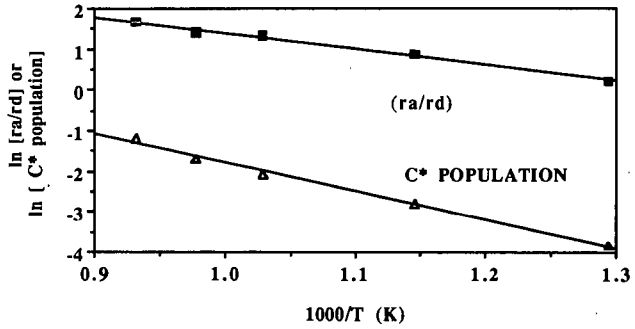

Figure 3. The variation of relative rates of rapid turnover and desorption processes with temperature, and the variation of rapid turnover site population with temperature. Values obtained from TGA experiments at 1 to 10 kPa NO pressure.

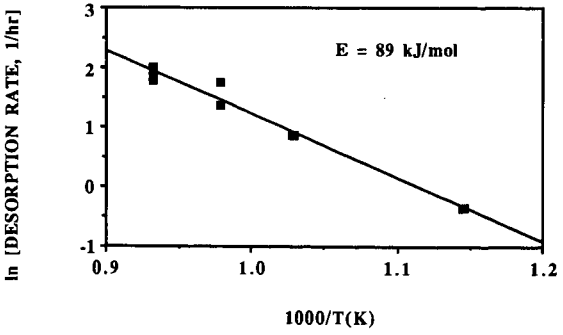

Figure 4. Oxide desorption rate, after removal of NO from the TGA.

NO RELEASE FROM THE ISOTHERMAL COMBUSTION OF COAL CHARS.

A.W. HARDING, S.D. BROWN and K.M. THOMAS.
Northern Carbon Research Laboratories, Department of Chemistry, Bedson Building, University of Newcastle upon Tyne, Newcastle upon Tyne, NE1 7RU, U.K..

Keywords: Char, combustion, gasification, NOx

Introduction

Coal combustion for power generation has associated environmental problems, in particular, the release of oxides of sulphur and nitrogen which are involved in the formation of acid rain [1,2]. The modification and optimization of the combustion process to minimise the NOx emissions is therefore of considerable interest and importance. The combustion of coal occurs over two stages;

1) the rapid devolatilisation followed by combustion/ignition of the volatiles *and*
2) slower gasification of the residual char.

The nitrogen present in the coal is partitioned between the volatile matter and the residual char. Char nitrogen has been identified [3] as the main contributor to NO emissions from low NO_x burners. Previous work on the gasification of char nitrogen [4-6] concentrated on temperature programmed conditions and possible mechanisms of the release of nitrogen. Carbons derived from polynuclear heterocyclic aromatic hydrocarbons with well defined initial functionality [7-10] and isotopic carbon (^{13}C) [11,12] were also used as models for char gasification.

In the present investigation, the release of NO during isothermal combustion of a suite of coal chars produced from a rank series of coals in an entrained flow reactor under conditions similar to those in pulverised fuel combustion systems was studied. The relationships between coal and char structural characteristics and NO release were investigated.

Experimental

Coal Samples

Twenty coals were used in the study, covering a wide range of rank from anthracite to high volatile bituminous coal.

Char sample preparation in an Entrained Flow Reactor(EFR)

Pyrolysis of the coal size fraction (38 - 75μm) to produce char samples was achieved by the injection of coal into an entrained-flow reactor at 1273K in a nitrogen atmosphere. The reactor had a zone length of 1.66m and the particles experienced residence times of ~1s. Char samples were collected using a water cooled probe and a cyclone.

Char characterisation data

Carbon, hydrogen and nitrogen contents were determined using a Carlo Erba 1106 elemental analyser. Proximate analyses of the chars were determined by modified thermogravimetric analysis using a Stanton Redcroft ST780 thermogravimetric analyser. Surface area measurements were obtained from CO_2 adsorption measurements at 273K in a McBain spring gravimetric apparatus.

Combustion measurements

A Thermal Sciences STA 1500 thermogravimetric analysis instrument was connected to a VG quadrupole 300 amu mass spectrometer via a 1mm i.d. silica lined stainless steel probe. The probe was placed directly above the sample at a distance of 10mm from the surface of the sample. Isothermal combustion was carried out by heating the sample to the desired temperature (873 - 1323K) in an atmosphere of argon. After thermal equilibrium was reached, the gas was switched to 20% oxygen/argon. A gas flow rate of 50 cm^3 min^{-1} was used with ~5mg of char sample with particle size 38-75μm. The gaseous species evolved and the weight loss profile were recorded with respect to time. Reactivity measurements were determined from isothermal gasification in 20% O_2/Ar at 773K. The reactivities of the chars during combustion were calculated from the rectilinear region of the weight loss-time curve.

Results

Isothermal Gasification measurements

The gasification rates of the coal chars at various temperatures between 773 and 1323K are shown in Figure 1 as a function of isothermal gasification temperature and volatile matter of the parent coal. It is apparent that there are two regions corresponding to the reaction being under chemical control at temperatures typically less than 973K, while above 973K the reaction is under diffusion control. In the chemical control region (below 973K), the gasification rate increases markedly with temperature. In the diffusion controlled region, above 973K, there is a very slow increase in the rate of gasification with temperature. In the region where the reaction is under chemical control, the gasification rate increases quite sharply with decreasing rank. In the region where the reaction is under diffusion control, there is a slight decrease in the gasification rate with coal rank.

Conversion of char nitrogen to NO

Isothermal Combustion profiles

Figure 2 shows the isothermal combustion profiles for a low rank coal char at 873 and 1273K in 20% O_2/Ar. At 873K, the combustion takes place where the reaction is under chemical control while at 1273K, the reaction is under diffusion control. It is evident that the NO/(CO + CO_2) ratio increases with increasing burn-off for combustion at both temperatures. Similar trends were observed for the combustion of the suite of chars under both chemical and diffusion control.

Gas concentration measurements

The release of nitric oxide from the combustion of the E.F.R. coal chars varied with the rank of the parent coal and the isothermal gasification temperature. In regions of low gasification temperature and for high rank coals, the ratio of nitric oxide released normalised to the initial amounts of nitrogen in the char (NO/char-N), was highest. For low rank coals, the effect of temperature on the NO/char-N ratio was not as great. It was also apparent that there was a dependence of the NO/char-N ratio on coal rank at any given temperature. There was a marked decrease in the NO/char-N ratio with a decrease in coal rank. Again, this was less apparent at the higher combustion temperatures when the reaction was under diffusion control.

The relationships between carbon structural characteristics and the conversion of char nitrogen to NO during combustion are of considerable interest. At low temperatures, gasification rate is governed by chemical control, and therefore the porous and surface structure of the char need to be taken into consideration. Figure 3 shows that there is a correlation between gasification

rate and the evolution of char-N as NO at 873K (chemical control region). At 1273K, when the reaction is under diffusion control, there was no correlation between char gasification rate and NO evolution. The clear correlation of NO/char-N with gasification rate observed for isothermal combustion at 873K was less evident when the rate was normalised by the surface area of the char. This indicates that the porous structure is a factor which influences the gasification of the char under chemical control and also the conversion of char-N to NO during combustion. In diffusion control, the external surface of the char is the important parameter.

Discussion

Char nitrogen conversion to NO

In this study, the gas sampling probe to the mass spectrometer was placed directly above the sample and this has been shown to detect reactive intermediate species before they are converted to equilibrium species (direct sampling) [6,10]. When the sampling probe is moved to the exhaust of the TGA, near equilibrium conditions are obtained (exhaust sampling). At this sampling position, the NO/N ratio increases due to small amounts of reactive intermediate species, such as HCN and $(CN)_2$ produced in the char gasification being converted to NO in the gas phase by reaction with oxygen [10]. NO is the major primary product of char-N gasification. Mass transport effects and reduction of the NO in the carbon bed in the TGA may also modify the conversion of char nitrogen to NO during gasification/combustion. Figure 2 shows that the $NO/(CO + CO_2)$ ratio increases with increasing carbon conversion and similar results were obtained for the combustion of the suite of chars under both chemical and diffusion control conditions. This can be attributed to two reasons; a) the retention of nitrogen in the char and/or b) the lower extent of reduction of the primary char nitrogen oxidation product NO, in the pores or on the surface of the char as the structure changes with carbon conversion.

Tullin *et al* have proposed [13] that char nitrogen reacts with either oxygen to form NO or with NO to form N_2O as the char undergoes gasification. The NO and N_2O are reduced by the char to N_2. Since the diameter of the char particles decreases with increasing carbon conversion there is less opportunity for the NO to be reduced. This explains the increase in $NO/(CO + CO_2)$ with increasing carbon conversion. These authors also observed a decrease in N_2O with carbon conversion. They proposed that there was a decrease in NO concentration in the pores, thus causing a reduction in the formation of N_2O. These authors used modelling studies [14] to support the proposal.

Previous studies of the isothermal combustion of model carbons prepared by the high pressure carbonization of polynuclear aromatic hydrocarbons gave similar results [7-9]. In addition, analytical data showed that the N/C ratio increased with increasing carbon conversion thereby supporting the former explanation. Therefore it is possible that both nitrogen retention and lower NO reduction occur with increasing carbon conversion.

Temperature programmed combustion studies of E.F.R. chars have shown [3,4] that the conversion of char-N to NO increases with rank up to ~ 1.5% vitrinite reflectance before reaching a plateau. High levels of NO release were also associated with lower reactivity chars and it was proposed that the char reactivity, total surface area, and char surface structure are factors which influence the conversion of char nitrogen to NO during combustion.

Previous studies have suggested that NO is reduced on the carbon surface to form N_2 and/or N_2O [4-8, 10, 13,14]. Also the CO reaction with NO may be catalysed by the char

surface [15]. High rank coals have a more ordered structure than the lower rank coals and there are generally fewer active sites available. In addition, the porous structure varies systematically with rank. Coals which develop thermoplasticity give rise to anisotropic chars where there is an increase in the extent of alignment of the carbon lamellae resulting in a low surface area. It is apparent that the coal chars which have the lower surface areas tend to be associated with higher levels of NO release. This indicates that the lower reactivity and available surface area of the high rank coal chars gives rise to higher NO/char-N conversion ratios due to a lower reduction of the primary char oxidation product NO on the surface and/or in the pores of the char. Figure 3 clearly shows that the less reactive chars are associated with high levels of NO release, at low temperatures where the reaction is under chemical control.

Conclusions

The release of nitrogen in the combustion of coal chars derived from a suite of coals covering a wide range of rank has been studied. The NO/(CO + CO_2) ratios increased with increasing burn-off for isothermal combustion in both the chemical and diffusion control temperature regimes. This suggests that the nitrogen is retained preferentially in the char and/or the extent of reduction of NO on the char surface is lower as carbon conversion proceeds. Lower conversions of char nitrogen to NO are observed from low rank coals. Chars with low surface areas and low reactivity have high conversions of char-N to NO. The primary product of char-N combustion, NO, is reduced in the porous structure and/or on the surface of the coal char. The char structure may also catalyse the reaction of CO with NO. The extent of reduction varies with temperature and mass transport limitations as well as the structure of the char.

References

1. Sloss,L.L.,*NOx Emissions from Coal Combustion,* IEACR/36,1991, IEA Coal Research, London.
2. Davidson,R.M. *Nitrogen in Coal,* IEAPER/08,1994,IEA Coal Research, London.
3. Phong-Anant, D., Wibberley, L.J. and Wall, T.F. *Combust. Flame* **62**, 21 (1985).
4. Wang, W., Brown, S.D., Hindmarsh, C.J. and Thomas, K.M. *Fuel* **73**, 1381 (1994).
5. Brown, S.D. and Thomas, K.M. *Fuel* **72**, 359 (1993).
6. Varey, J.E., Hindmarsh, C.J. and Thomas, K.M. *Fuel* accepted for publication.
7. Wang, W.and Thomas, K.M. Fuel **71**, 871 (1992).
8. Wang, W. and Thomas, K.M. Fuel **72**, 293 (1993).
9. Spracklin, C.J., Thomas, K.M., Marsh, H. and Edwards, I.A.S. *International Conference on Coal Science Proceedings,* IEA Coal Research, 1991, p. 343.
10. Jones, J.M., Harding, A.W., Brown, S.D. and Thomas K.M. *Carbon* **33**, 833 (1995).
11. Thomas, K.M., Grant, K. and Tate, K. *Fuel* **72**, 941 (1993).
12. Jones, J.M. and Thomas, K.M. *Carbon* **33**,1129(1995).
13. Tullin, C.J., Sarofim, A.F. and Beer, J.M. *J. Inst. Energy* **66**, 207 (1993).
14. Tullin, C.J., Goel, S., Morihara, A., Sarofim, A.F. and Beer, J.M. *Energy and Fuels* **7**, 796 (1993).
15. Goel,S.K.,Morihara,A. Tullin,C.J. and Sarofim,A.F., 25th Symp.(Int.) on Combustion, The Combustion Institute, Pittsburgh,1051(1994)

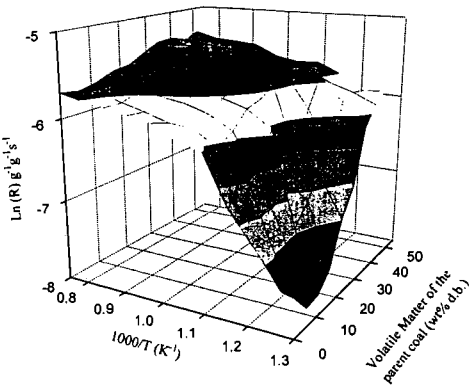

Figure 1. The variation of char reactivity with 1/T and volatile matter of the parent coal.

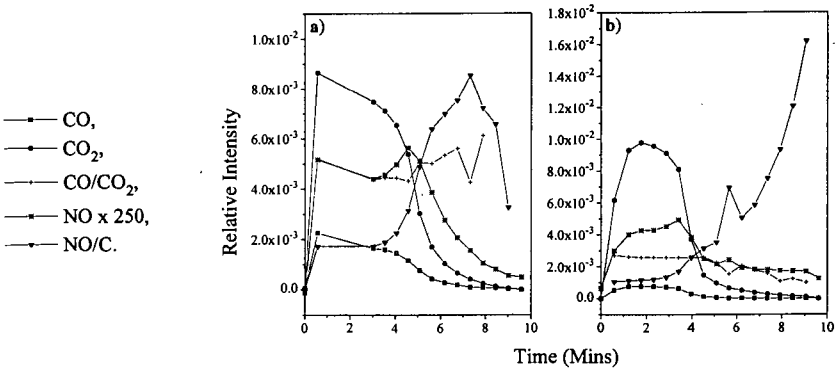

Figure 2. Gas evolution profiles from the isothermal combustion in 20% O_2/Ar of a) char-T at 873K, b) char-T at 1273K.

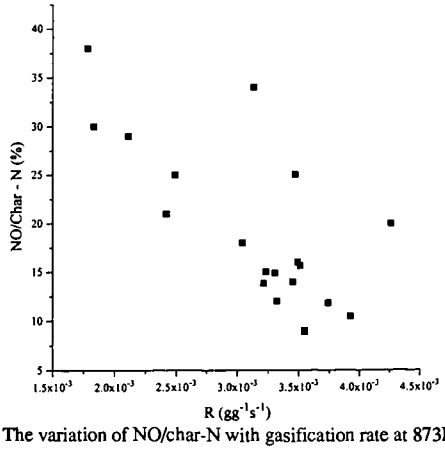

Figure 3. The variation of NO/char-N with gasification rate at 873K.

NO REDUCTION WITH CARBON — ANALYSIS OF REACTION MECHANISM BY USING ISOTOPICALLY LABELED NO —

Ph. Chambrion, H. Orikasa, T. Kyotani and A. Tomita
Institute for Chemical Reaction Science,
Tohoku University, Sendai 980, Japan

Keywords: Carbon; NO; Transient kinetics

ABSTRACT

The NO reduction with carbon has been investigated in the presence of oxygen. The use of both mass spectrometer and gas chromatography for gas analysis, together with the use of isotope gas, was quite powerful. It was concluded that N_2 was formed by the reaction between surface nitrogen species and gaseous NO.

INTRODUCTION

Emission of nitrogen oxides is of concern from an environmental point of view as it may be involved in the formation of photochemical smog and acid rain. When they are produced by coal combustion or diesel engines, carbonaceous matter appears to be a good candidate as reducing agent, producing N_2, CO and CO_2[1,2]. However, oxygen is usually present and particular attention was recently paid to the role it plays in the reduction of nitrogen oxides[3,4]. These studies clarified the function of oxygen-containing complexes on carbon as reaction intermediates. The presence of nitrogen-containing species at the surface of carbon was also revealed but the species appear to be stable until 1000°C, at least in the absence of oxygen[2,5].

The purpose of this study is to investigate the role of nitrogen containing species trapped on the carbon surface in the reduction of NO with carbon in the presence of oxygen.

EXPERIMENTAL

Phenol formaldehyde resin (PF) char is used as carbon source throughout this study. Its preparation was described in details in a recent publication[4]. In a typical experiment, about 200 mg of PF char was placed in a fixed bed reactor under He flow and then heat-treated at 950°C for 30 min immediately before use. The concentration of reactant gas was normally around 500 ppm of NO and 5 % of O_2 both diluted in He. $^{15}N^{18}O$ gas was purchased from Isotec Co. and its isotopic purity is 99 % for N and 95 % for O. Neither isotopically labeled carbon nor O_2 were used in this study.

Gases emitted during experiments are identified and quantified simultaneously by mass spectrometer (MS: Anelva AQA 200) and gas chromatography (GC: Area M200). For GC analysis, MS5 and PPQ columns were used for the separation of O_2, N_2 and CO and for CO_2, respectively. Both MS and GC were calibrated by using commercially available standard gases diluted in He.

RESULTS AND DISCUSSION

NO conversion in TPR experiment.

Temperature programmed reactions (TPR) of PF char in the presence of 420 ppm NO were carried out at a rate of 3°C·min^{-1} (Figure 1). Without O_2, the reaction began at about 600°C and almost completed at 950°C. In the presence of oxygen (2 vol%), NO conversion started at 200°C but remained lower than 5 % up to 450°C. Thereafter, it increased to be completed at 700°C. Thus, O_2 shifted the conversion curve of NO by more than 200°C. It should be noteworthy that O_2 conversion curve coincided with that of NO. This coincidence was also observed for other carbon samples, brown coal char, activated carbon and graphite, in spite that the reaction started at quite different temperatures for these four carbons. The reaction with O_2 might create reactive sites which are able to react with NO[2]. In the following experiments 600°C was chosen as the reaction temperature, since this is low enough to avoid an excess reaction of NO in the presence of O_2 and high enough to obtain reasonable conversion rate without O_2.

Reduction of NO at 600°C in the absence of O_2.

Conversion curve in Figure 1 indicates that NO reduction on PF char is almost negligible at 600°C in the absence of O_2. However, since pretreatment by oxygen creates reactive sites available for NO reduction, PF char pretreated by 5 % O_2 at 600°C for 20 min was used to react with 530 ppm NO. Figure 2 shows that before introduction of NO into the reactor, only residual evolution of CO was noticed, indicating the desorption of oxygen complexes from the pretreated char. Introduction

of NO was immediately followed by a dramatic increase of CO production as well as CO_2 and N_2. This indicates the effective reduction of NO even in the absence of O_2. The presence of oxygen-containing sites in char play a key role in this reaction. Thereafter, products concentration decreased to stabilize as NO conversion decreased to a quasi-steady state. After 15 min of the reaction, NO concentration was about 350 ppm in the exhaust gas, corresponding to NO consumption of 180 ppm. N_2 production did not exceed 15 ppm, suggesting the storage of nitrogen species in char. Such compounds are known to be stable, at least under an inert atmosphere to 1000°C[2,5].

Reaction of PF char with NO was immediately followed by its TPR at 10°C·min^{-1} in the presence of 5 % O_2. Figures 3a and 3b show gas evolution during this TPR. The conversion of O_2 started at 500°C (Figure 3a). CO concentration increased first to reach a maximum at 680°C and then decreased while CO_2 reached two maxima at 680 and 830°C and thereafter decreased as the amount of carbon remaining in the reactor became too small. N_2 and NO production profiles were shown in Figure 3b. It seems natural that a part of nitrogen species on PF char, produced in the preceding NO reaction, was oxidized by O_2 and converted to NO. Interestingly, as was reported in the previous paper[4], the formation of N_2 was observed in spite that only O_2 was present as a reactant. Nitrogen containing surface species was liberated as N_2 with the aid of oxygen. It should be noted that the use of both MS and GC made this observation possible.

Reduction of NO at 600°C in the presence of O_2 — Transient kinetics.

In order to clarify whether N-containing species are involved in NO reduction on PF char or not, the following transient kinetic experiment was done: a mixture of 530 ppm $^{14}N^{16}O$ and 5 % O_2 was flowed through the reactor at 600°C for 21 min and then switched to a flow of 530 ppm $^{15}N^{18}O$ and 5 % O_2 for additional 21 min. The main products were CO and CO_2. First, as shown in Figure 4a, their concentrations increased together with O_2 conversion. This may be related to the activation of PF char. Thereafter, concentrations stabilized and later CO and CO_2 production slowly decreased perhaps because of the loss of carbon. Species produced in lower amounts are presented in Figure 4b. First, the conversion of NO to N_2 increased accompanied with the activation of PF char. NO concentration in this steady state was around 370 ppm, which corresponded to disappearance of about 160 ppm. As N_2 concentration did not exceed 35 ppm, some accumulation of nitrogen in PF char might have taken place during this period.

Switching from $^{14}N^{16}O$ to $^{15}N^{18}O$ resulted in a sudden decrease in $^{14}N^{16}O$, and various products were formed. Main products were $C^{16}O$ and $C^{16}O_2$ (Figure 4a) with some $C^{16}O^{18}O$ (Figure 4b). As nitrogen-containing species, m/e of 29, 30, 31 and 33 were observed and they were assigned to $^{14}N^{15}N$, $^{14}N^{16}O$ or $^{15}N_2$ (or $C^{18}O$), $^{15}N^{16}O$ and $^{15}N^{18}O$, respectively. The most important observation here is the formation of $^{14}N^{15}N$. The concentration of $^{14}N^{15}N$ was almost the same as the amount of N_2 determined by GC at least in the initial stage of $^{15}N^{18}O/O_2$ gasification. This indicates that the main N_2 species was $^{14}N^{15}N$, and the formation of $^{14}N_2$ (the same m/e with $C^{16}O$) and $^{15}N_2$ (the same m/e with $C^{18}O$ and $^{14}N^{16}O$) was negligible. In the later stage, however, the discrepancy between $^{14}N^{15}N$ and N_2 (by gas chromatography) became apparent, and therefore $^{15}N_2$ might contribute to some extent in this region. This can be interpreted by the depletion of ^{14}N-species and accumulation of ^{15}N-species on carbon. The above observation suggests that the N_2 formation mechanism can be related to the interaction between ^{14}N-species previously kept in PF char and $^{15}N^{18}O$ in gas phase.

$$C(^{14}N) + {}^{15}NO \text{ -----> } {}^{14}N^{15}N + CO_x + C_f$$

In the previous study[1], it was shown that the possibility of the above mechanism was rather small. However, the previous results were obtained in the absence of oxygen, where the formation rate of N_2 was very low. Moreover, the char was treated for 1 h with He prior to the reaction with NO, and thus the surface nitrogen species was stabilized to some extent. Therefore the present condition is different from that reported earlier and it is more close to the actual gasification condition of interest.

The total NO concentration at 40 min can be expected at around 300 ppm from the extrapolation of the NO concentration between 0 and 21 min, since the reaction itself was continuous before and after gas switching. Unreacted $^{15}N^{18}O$ was 120 ppm and $^{15}N^{16}O$ produced by isotope exchange was 110 ppm. The rest should be $^{14}N^{16}O$ which is the reaction product between surface ^{14}N and gaseous $^{16}O_2$. Gases for m/e of 46, 30 and 31 evolved rather slowly in the beginning, because accumulation of new surface species by the reaction with $^{15}N^{18}O$ was necessary for the formation of these gases.

CONCLUSION

Use of GC and MS enables to show the gas formation behavior in detail during the NO reduction with carbon in the presence of oxygen. Nitrogen-containing species previously trapped on PF char was removed as either N_2 or NO during TPR in O_2. The transient kinetic study where $^{14}N^{16}O$ was switched to $^{15}N^{18}O$ in the presence of $^{16}O_2$ clearly showed the formation of $^{14}N^{15}N$. This is a strong evidence for the proposed mechanism of N_2 formation, which involves one nitrogen from surface nitrogen-containing species and another nitrogen from gaseous NO.

REFERENCES

1. Orikasa, H., Suzuki, T., Kyotani, T., Tomita, A., Martin, R. R. *22nd Biennial Conference on Carbon*, San-Diego, 1995, pp. 626-627.
2. Teng, H., Suuberg, E. M., Calo, J. M. *Energy Fuels* 1992, **6**, pp. 398-406.
3. Yamashita, H., Tomita, A., Yamada, H., Kyotani, T., Radovic, L. R. *Energy Fuel* 1993, **7**, pp. 85-89.
4. Suzuki, T., Kyotani, T., Tomita, A. *Ind. Eng. Chem. Res.* 1994, **33**, pp. 2840-2845.
5. Kapteijn, F., Pels, J.-R., Moulijn, J. A., Zhu, Q., Thomas, K. M. *22nd Biennial Conference on Carbon*, San-Diego, 1995, pp. 548-549.

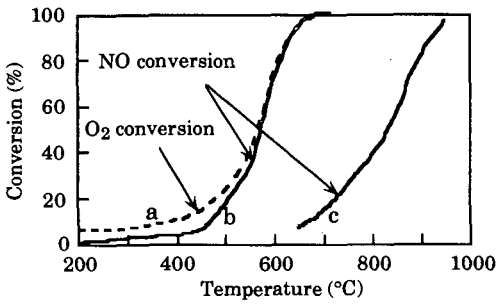

Figure 1 Gas conversion in the presence of PF char. Reactant gas: (a,b) 420 ppm NO+ 2 % O_2, (c) 420 ppm NO.

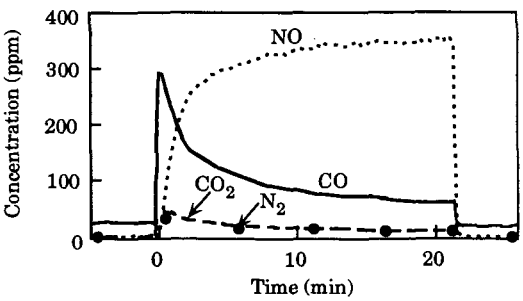

Figure 2 Gas evolution during NO reaction with PF char pretreated with O_2. Solid marks refer to N_2 concentration determined by GC.

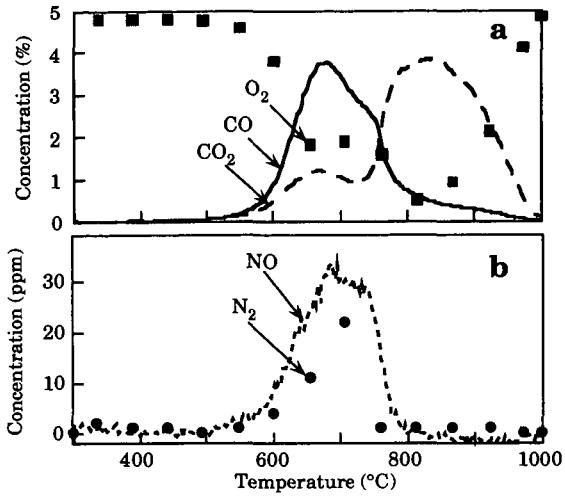

Figure 3 TPR pattern of PF char in the presence of 5 % O_2. (a) O_2, CO and CO_2, (b) NO and N_2. Solid marks refer to concentration determined by GC.

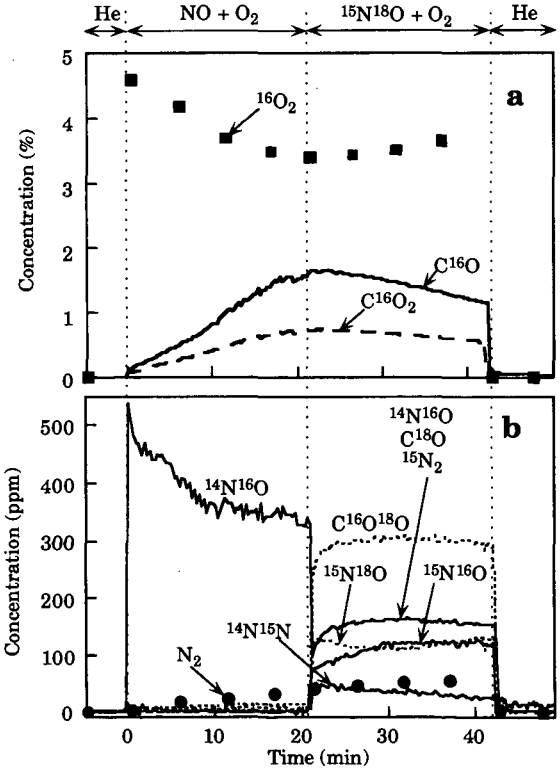

Figure 4 TK pattern on switching from $^{14}N^{16}O$ to $^{15}N^{18}O$ in the presence of 5 % $^{16}O_2$. (a) $^{16}O_2$, $C^{16}O$ and $C^{16}O_2$; (b) N_2, $^{14}N^{15}N$ and other gases. Solid marks refer to concentration determined by GC.

REDUCTION OF NITRIC OXIDE BY LOW-RANK COAL CHARS

M. J. Illán-Gómez, C. Salinas-Martínez de Lecea*, A. Linares-Solano*, J. Phillips and L. R. Radovic**

Fuel Science Program and **Department of Chemical Engineering
The Pennsylvania State University, University Park, PA 16802
***Departamento de Química Inorgánica, Universidad de Alicante, Spain**

KEYWORDS: coal, char, nitrogen oxides, reduction.

INTRODUCTION

The increasingly stringent environmental legislation requires efforts to find more effective and inexpensive pollution control systems. Removal of NO_x from both stationary and mobile sources is the subject of very intense research and development. Selective catalytic reduction (SCR) is commercially available technology [1,2]. However, when excess oxygen is present in the exhaust gases the state-of-the-art catalyst is not effective for removing NO_x [3-5].

Carbon is known to be an effective adsorbent and catalyst in the simultaneous removal of SO_x and NO_x [6-8]. Reducing agents such as NH_3, CO, H_2 or hydrocarbons with an alumina- or titania-supported catalyst are used [3,9-10]. The problem with this technology is the need to introduce a reducing agent to the feed. The use of inexpensive coal-based chars which are gradually consumed can be an interesting solution because no additional reductant is required. Chars produced from lignites are known to exhibit high catalytic activity for the reduction of NO with ammonia [11] and recently a 'calcined' char from a subbituminous coal was used to remove NO_x with the assistance of microwave energy [12].

In this paper, low-rank coal chars are used to remove NO_x from an oxygen-rich atmosphere. The effects of both pyrolysis temperature and inorganic impurities naturally present in coals are studied.

EXPERIMENTAL

Four low-rank coals, two lignites and two subbituminous coals, were selected for direct NO reduction in the presence of O_2. Table 1 shows the PSOC number, the ASTM rank and selected inorganic components in the coals. Eight chars were obtained by pyrolyzing the coals in a tube furnace at 500 and 700 °C (N_2, 80 mL/min, 1h). An additional char was prepared by pyrolyzing one of the lignites at 900 °C.

The kinetics of the $NO+O_2$/carbon reaction was studied at atmospheric pressure in a fixed-bed quartz microreactor connected to a quadrupole mass spectrometer (VG QUADRUPOLE). Temperature-programmed reaction ($^{15}NO+O_2$, 10 °C/min, T_{max}=500 °C) and isothermal reaction experiments were carried out in the following environments: (i) 0.5% ^{15}NO/Ar, (ii) 5% O_2/Ar, and (iii) 0.5% ^{15}NO/5% O_2/Ar. Temperature-programmed desorption (TPD) runs were also conducted (He, 20 °C/min, T_{max}=900 °C) before and after isothermal reaction in the various mixtures.

RESULTS AND DISCUSSION

Temperature-programmed reaction (TPR) experiments. Figure 1 shows the TPR curves, %NO reduction *vs.* reaction temperature, for the three chars obtained from lignite 1422. Chars 1422/700 and 1422/900 exhibit somewhat different behavior from that of the low-temperature char (1422/500): NO reduction maximum at low temperature (T<200 °C) and a lower NO reduction capacity at high temperature (T>200 °C). As can be concluded from Figure 2, this characteristic low-temperature TPR profile is only exhibited by chars prepared from lignites 1422 and 1548, which have the highest potassium and sodium content (see Table 1). Similar low-temperature profiles were found for activated carbon loaded with potassium [13,14].

The analysis of reaction products evolved during the low-temperature reaction stage reveals some significant differences with respect to the potassium-loaded activated carbons. The quantity of N_2 evolved is much smaller than the quantity of NO retained (~5%); in other words, non-dissociative NO chemisorption seems to be the main phenomenon occurring at the low temperatures [13,14]. Subsequent desorption of thus retained NO gives rise to the negative values shown at intermediate temperatures in Figures 1 and 2.

The fact that the low-temperature TPR behavior described above is observed only for chars pyrolyzed at 700 and 900 °C means that important changes take place during the coal pyrolysis step. The theoretical temperature of reduction of potassium oxide (K_2O) by carbon (graphite) is 825 °C [15]; furthermore, it is well known [16] that reduced potassium species can spread over the surface and thus achieve a high degree of dispersion. Obviously, these two phenomena are more important at higher pyrolysis temperatures; consequently, potassium-catalyzed NO adsorption [17] becomes more pronounced.

In the high-temperature region, where a continuous increase in NO reduction is observed (Figures 1 and 2), pyrolysis temperature has the opposite effect: the low-temperature char exhibits a higher activity for NO reduction than chars pyrolyzed at higher temperatures (1422/700 and 1422/900). Analysis of the reaction products evolved shows that NO reduction is accompanied by evolution of N_2, N_2O and CO_2.

Char 1422/500 thus shows the highest activity for NO reduction. In agreement with the well known effects of pyrolysis temperature on char reactivity [18-20], it also has the highest reactivity in O_2 (see also Table 2). For example, the temperature at which the O_2/C reaction starts (during a TPR experiment) is the lowest. Also, the ignition temperature has been used in the literature as a good index to compare the reactivity of carbons in O_2 [21]; lower ignition temperature was observed for char 1422/500 (~305 °C) than for char 1422/700 (~340 °C). On the other hand, a higher ignition temperature and no substantial difference was observed for the two chars prepared from coal 1547 (~380 °C for both 1547/500 and 1547/700), which has the lowest content of potassium and sodium. This is not a surprising result of course. Alkali metals are very effective catalysts for carbon oxidation reactions [22]. Furthermore, a correlation between the NO reduction capacity of a char and its reactivity in O_2 has been discussed in detail recently [17].

It was thus of interest to monitor the nature and quantity of carbon-oxygen surface complexes formed on the surface of room-temperature-air-exposed coal chars before NO reduction. The CO_2 and CO evolved in a TPD experiment is a convenient measure of surface complexes present on the chars [23]. The quantity of CO_2 and CO evolved by the low-temperature char 1422/500 (1605 and 650 μmol/g C) is higher than that evolved from high-temperature chars 1422/700 and 1422/900 (902 and 963 μmol/g C, and 369 and 113 μmol/g C, respectively); furthermore, the chars obtained from subbituminous coals, 1547/500 and 1547/500, yield less CO_2 and CO (703 and 928 μmol/g C, and 549 and 386 μmol/g C, respectively).

The different effects of pyrolysis temperature in the low-temperature *vs.* high-temperature region imply that different active sites are involved in the two regimes. At low temperatures, the activity for NO reduction is governed by the catalyst active sites; at higher temperatures, the reactivity of the char (i.e., the number of carbon active sites) appears to control the NO reduction behavior. A similar conclusion was reached in our previous TPR study using an activated carbon loaded with different amounts of potassium: the low-temperature profile was determined by catalyst loading and dispersion, but no differences were observed at higher temperatures, where carbon reactivity controls the NO reduction capacity [14].

Isothermal reaction experiments. Isothermal reaction experiments were performed in three different atmospheres: NO+O_2, NO and O_2. After reaction (for ca. 60 minutes), a TPD experiment was also performed.

Figure 3 shows the evolution of the % NO reduction curve with time for all chars pyrolyzed at 500 °C and also for chars 1422/700 and 1422/900. Table 2 summarizes the kinetic data for NO reduction after 1 hour in both atmospheres (NO and NO+O_2), as well as the reactivity in oxygen (5% O_2, balance Ar) and the level of carbon consumption (% burnoff). The isothermal behavior observed supports the conclusions based on the TPR study: (a) chars from lignites 1422 and 1548 have a higher capacity for NO reduction than chars prepared from subbituminous coals, and (b) the low-temperature chars show the highest activity in the NO+O_2/C reaction. Table 2 also reveals that the high NO reduction level is maintained by chars 1422/500 and 1548/500 and that a reasonable carbon consumption level is achieved. The main reaction products are N_2 and CO_2, with some N_2O being evolved (N_2O/N_2=0.15), but CO is not detected.

The activity data in the absence of oxygen confirm the important enhancement of NO reduction capacity in an oxygen-rich atmosphere [24,17]. The degree of enhancement is larger for the 500 °C chars than for the 700 °C chars. It is also more important for chars obtained from the two lignites. The reactivity in O_2 seems to be the key to the understanding of these effects: chars that exhibit the highest increase in NO reduction (1422/500 and 1548/500) also have the highest reactivity in oxygen. Again, the analogy between NO reduction by carbon and the carbon/O_2 reaction is made apparent.

The results discussed above are in agreement with some recent studies of Tomita and coworkers [25] and with our previous proposal about the role of oxygen in NO reduction [17]. This can be summarized succinctly as follows:

$$2C_f + O_2 \longrightarrow 2C(O) \quad (1)$$

$$2C(O) \longrightarrow CO_2 + C_f \quad (2)$$

$$C(O) \longrightarrow CO\,(+\,C_f) \quad (3)$$

Upon desorption of CO_2 and CO, a larger number of free actives sites (C_f) on the carbon surface is produced than in the absence of O_2; it is these 'nascent' sites which increase char's activity for NO reduction. By comparing columns 3, 5 and 7 in Table 2, we conclude that, despite the much higher propensity of chars to react with O_2, the fraction of carbon consumed by NO (column 8) can be quite high. (It is this number which may require some additional optimization in pursuit of commercial viability of this novel approach to NO_x reduction.) Mochida et al. [26] recently concluded also that the active sites in carbon/NO/O_2 system are created by liberation of CO and CO_2, in contrast to their earlier assumption [7] that the active sites are the carbon-oxygen surface complexes.

Finally, analysis of the species evolved during TPD after isothermal reaction also provides valuable information. Evolution of N_2 is not significant, suggesting both that N_2 is produced primarily according to the reaction $2NO + 2C_f = 2C(O) + N_2$ [17] and that the concentration of C(N) surface complexes is not very high. This conclusion is in agreement with our previous results using activated carbons [13-14,17,27]. In Figure 4, the increase in the amount of CO_2 evolved after the NO+O_2/C reaction indicates that some oxygen is retained on the surface during the NO/C reaction. This surface oxygen (or oxygen-containing species) can be retained by either the catalyst or the char. The fact that the CO_2 desorption curves show a peak with a maximum at ~560 °C suggests that CO_2 is captured by K_2O thus forming a carbonate. The formation of K_2CO_3 has also been suggested by García-García et al. [28] after the NO+O_2/C reaction in similar potassium-loaded char samples; its decomposition, during subsequent TPD, exhibited a maximum at ~600 °C. The CO curves show a maximum at ~700 °C, which can be due to partial reduction of metallic oxides present in the ash (e.g., K_2O, Na_2O, Fe_2O_3) by the char. (CO peaks with maxima at ~750 and ~800 °C were observed during TPD of K- and Fe-loaded activated carbons [13,27].) In support of the above interpretation is the finding that TPD curves for chars 1422/700 and 1422/900 show a better defined CO_2 peak after NO+O_2/C and O_2/C reactions, even though a lower amount of CO_2 is evolved (in agreement with the fact that these chars are less active for NO reduction): a more reduced and better dispersed potassium species seems to be obtained after pyrolysis at 700 and 900 °C. Another interesting result from this series of TPD experiments is that the amount of CO_2 retained by the char after NO+O_2/C reaction increases with increasing pyrolysis temperature: 4% of CO_2 evolved is captured (as K_2CO_3) by char 1422/500, while 18 and 55% are captured by chars 1422/700 and 1422/900, respectively.

ACKNOWLEDGEMENTS

This study was made possible by financial support from the U.S. Department of Energy (Grant No. DE-FG22-95PC95225) and a postdoctoral grant for MJIG from the Ministry of Science and Education of Spain. Coals from the Penn State/DOE (PSOC) sample and data bank were provided by D. Glick.

REFERENCES

1. Cho, S.M. *Chem. Eng. Prog.*, January 1994, p. 39.
2. Jüntgen, H.; Kühl, H. In *Chemistry and Physics of Carbon* (P.A. Thrower, Ed.), Marcel Dekker, New York, 1989, Vol. 22, p. 145.
3. Bosch, H.; Janssen, F. *Catal. Today* **1987**, *2*, 369.
4. Kapteijn, F.; Stegenga, S.; Dekker, N.J.J.; Bijsterbosch, J.W.; Moulijn, J.A. *Catal. Today* **1993**, *16*, 273.
5. Burch, R.; Millington, P.J.; Walker, A.P. *Appl. Catal. B* **1994**, *4*, 65.
6. Knoblauch, K.; Richter, E.; Jüntgen, H., *Fuel* **1981**, *60*, 832.
7. Mochida, I.; Ogaki, M.; Fujitsu, H.; Komatsubara, Y.; Ida, S. *Fuel* **1985**, *64*, 1054.
8. Kusakabe, K.; Kashima, M.; Morooka, S.; Kato, Y. *Fuel* **1988**, *67*, 714.
9. Harrison, B.; Wyatt, M.; Gough, K.G. *Catalysis* (London) **1982**, *5*, 127.
10. Armor, J.N. *Appl. Catal. B* **1992**, *1*, 221.
11. Lee, J.K.; Suh, D.J.; Park, S.; Park, D. *Fuel* **1993**, *72*, 935.
12. Cha, C.Y.; Kong, Y. *Carbon* **1995**, *33*, 1141.
13. Illán-Gómez, M.J.; Linares-Solano, A.; Radovic, L.R; Salinas-Martínez de Lecea, C. *Energy Fuels*, **1995**, *9*, 97.
14. Illán-Gómez, M.J.; Linares-Solano, A.; Radovic, L.R; Salinas-Martínez de Lecea, C. *Energy Fuels*, **1995**, *9*, 104.
15. Gilchrist, J.D. "Extraction Metallurgy", 2nd Ed. (Inter. Ser. Mater. Sci. Technol., Vol. 30), Pergamon Press; Oxford, UK, 1980.
16. Pullen, J.R. *Catalytic Coal Gasification*, IEA Report ICTIS/TR26, Coal Research, London, 1984.
17. Illán-Gómez, M.J.; Linares-Solano, A.; Radovic, L.R; Salinas-Martínez de Lecea, C. *Energy Fuels*, in press (to be published in January/February 1996).
18. Jenkins, R.G.; Nandi, S.P; Walker, Jr., P.L. *Fuel* **1973**, *52*, 288.

19. Radovic, L.R.; Walker, Jr., P.L.; Jenkins, R.G. *Fuel* **1983**, *62*, 849.
20. Zhang, L.; Calo, J.M.; Lu, W. This meeting (March 1996).
21. McKee, D.W. In *Chemistry and Physics of Carbon* (P.L. Walker, Jr. and P.A. Thrower, Eds.), Marcel Dekker, New York, 1981, Vol. 16, p. 1.
22. Kapteijn, F.; Moulijn, J.A. *Fuel* **1983**, *62*, 221.
23. Otake, Y.; Jenkins, R.G. *Carbon* **1993**, *31*, 109.
24. Yamashita, H.; Yamada, H.; Kyotani, T.; Radovic, L.R.; Tomita, A. *Energy Fuels* **1993**, *7*, 85.
25. Suzuki, T.; Kyotani, T.; Tomita, A. *Ind. Eng. Chem. Res.* **1994**, *33*, 2840.
26. Mochida, I.; Kisamori, S., Hironaka, M.; Kawano, S.; Matsumura, Y.; Yoshikawa, M. *Energy Fuels* **1994**, *8*, 1341.
27. Illán-Gómez, M.J.; Linares-Solano, A.; Radovic, L.R; Salinas-Martínez de Lecea, C. *Energy Fuels* **1995**, *9*, 112; *9*, 540.
28. García-García, A.; Illán-Gómez, M.J.; Linares-Solano, A.; Salinas-Martínez de Lecea, C., *Proc. 8th Internat. Conf. Coal Science*, Oviedo, Spain, 1995, p. 1787.

Table 1. Properties of Coals

PSOC No.	ASTM rank	ASTM ash yield (wt %)	Inorganic element analysis (wt %)
1422	Lignite	9.49	Na, 0.73; K, 0.11; Ca, 1.4; Fe, 0.81
1548	Lignite A	6.37	Na, 0.66; K, 0.05; Ca, 1.8; Fe, 0.61
1547	Subbituminous	9.85	Na, 0.12; K, 0.05; Ca, 1.3; Fe, 0.85
1546	Subbituminous	4.80	Na, 0.25; K, 0.05; Ca, 0.60; Fe, 0.20

Table 2. NO Reduction Data at 350 °C for Different Coal Chars

Char	Pyrolysis yield (wt %)	% NO reduced		% Burnoff		Reactivity in O_2 (h^{-1})*	F**
		$NO+O_2$	NO	$NO+O_2$	NO		
1422/500	45	54	12	19.5	0.3	0.20	0.13
1422/700	37	34	18	4.0	0.4	0.06	0.25
1422/900	32	0	-	1.1	-	0.01	0.23
1548/500	47	53	12	21.0	0.5	0.23	0.09
1548/700	40	35	15	4.0	0.4	0.04	0.37
1547/500	54	17	0	3.4	0.3	0.04	0.21
1547/700	52	11	10	2.6	0.2	0.02	0.22
1546/500	52	24	-	11.0	-	0.13	0.20
1546/700	45	11	-	4.3	-	0.05	0.27

*integrated value, based on carbon consumption over the 60-minute period.
**F = fraction of carbon consumed by NO (in the $NO+O_2/C$ reaction).

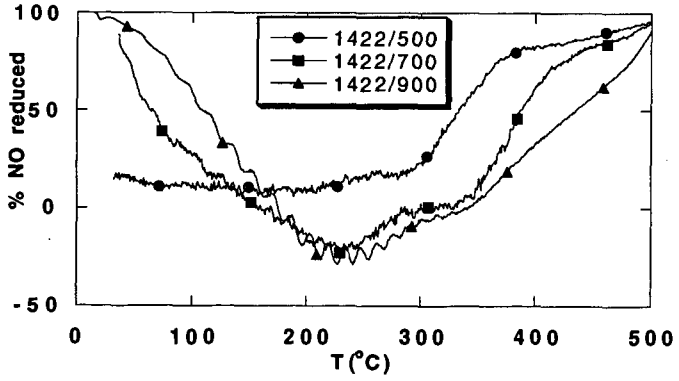

Figure 1. TPR profiles (0.5% NO, 5% O_2, balance Ar) for chars obtained from lignite 1422: effect of pyrolysis temperature.

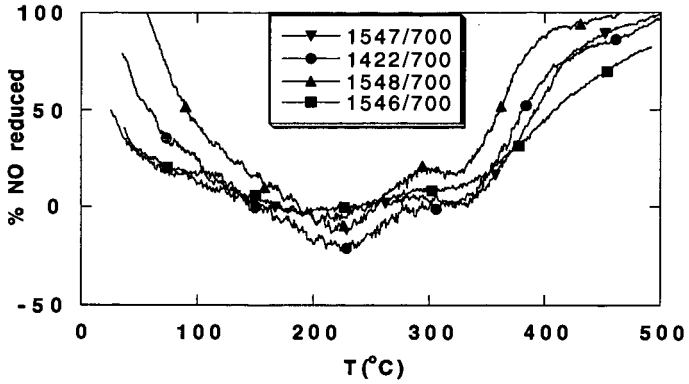

Figure 2. TPR profiles (0.5% NO, 5% O_2, balance Ar) for chars pyrolyzed at 700 °C: effect of coal rank.

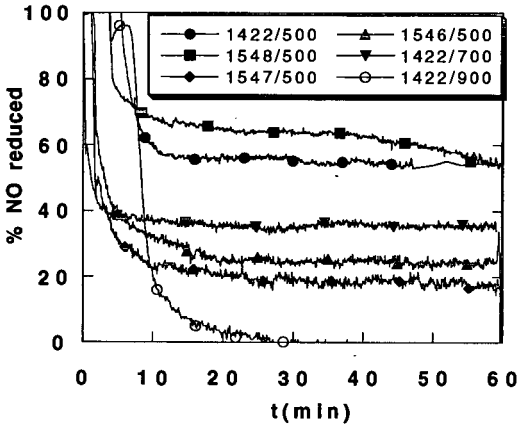

Figure 3. Effect of pyrolysis temperature on the kinetics of the NO+O_2/C reaction (350 °C; 0.5% NO, 5% O_2, balance Ar).

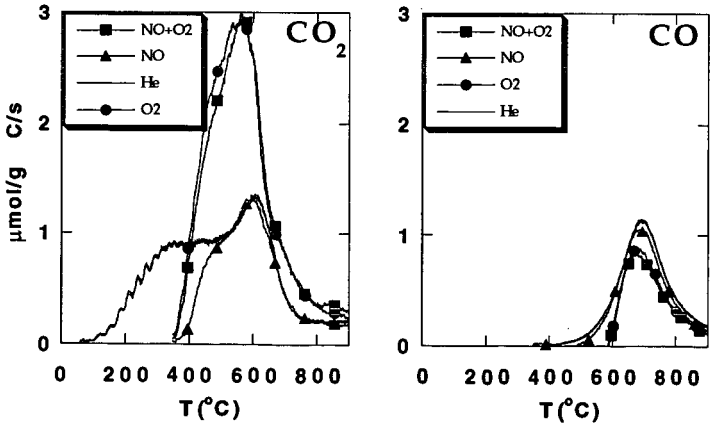

Figure 4. TPD profiles for sample 1422/500 before (He) and after reaction in NO+O_2, NO and O_2.

THE EFFECTS OF CaO CATALYSIS ON THE KINETICS OF NO REDUCTION BY BEULAH ZAP CHAR

Feng Guo and William C. Hecker *
Department of Chemical Engineering and Advanced Combustion Engineering Research Center (ACERC), Brigham Young University, 350 CB, Provo, Utah 84604

Keywords: NO/char reaction; Catalysis; Kinetics.

INTRODUCTION

The reduction of NO emissions from combustion processes has become increasingly important in protecting the world's environment. It has been shown that Selective Catalytic Reduction (SCR) with ammonia is an effective commercial technique to remove NO_x from combustion flue gas. However, the implementation of this technique is limited by high investment and operating costs, "ammonia slip", and SO_x poisoning, which motivate the search for alternatives.[1] Carbon (activated carbon or char) is a promising reducing agent for NO_x reduction with many potential advantages, such as low cost, easy availability, high efficiency, simplicity of process, and no secondary pollution.[1-7] Moreover, the heterogeneous reaction of NO with char is very important for the understanding of the formation of NO_x from coal combustion processes. The reaction may significantly destroy the NO_x formed earlier in coal combustion, which partially contributes to low NO emission from fluidized bed combustion.[2,3] Therefore, the reaction of NO with char is receiving significant attention in the literature.

Previous investigations on the reaction of NO with char involve the kinetics and mechanism,[6-23] the effects of char surface area, [24,25] the effects of feed gas composition,[10,7,25] and the catalytic effects of metals.[5,10,22,26-29] The reaction of NO with char has generally been reported to be first order with respect to NO partial pressure,[7,13-16] but reaction orders between 0.42 and 0.73 have also been reported.[30] A sharp shift in the activation energy has been observed in the temperature range of 873~973 K, which suggests a complex reaction mechanism.[6,7,15-18] Several mechanisms have been proposed.[5,6,12,16,18,19,25] However, questions concerning N_2 formation, the surface complexes, the nature of active surface sites, and the effects of minerals in char ash are still not well understood. In most previous studies, chars were taken to be pure carbon, thus the effects of the ash in chars and its composition on the kinetics and mechanism of the reduction reactions are not well known. Although the catalytic effects of certain metals or metal oxides on the reactions have been investigated,[5,10,22,26-29] little is known about their effects on the kinetics of the reaction. Therefore, the objectives of this study are to investigate the kinetics of the reaction of NO with Beulah Zap chars, to study the effects of CaO on the kinetics.

EXPERIMENTAL METHODS

The chars used in this study were prepared from 63 – 74 μm particles of North Dakota Beulah Zap lignite in a methane flat-flame burner (FFB). Parent char (NDL), a portion of NDL *washed* with HCl to remove mineral matter (NDW), and a portion of NDW *reloaded* with calcium oxide (NCa) were used. The CaO contents of NDL, NDW, and NCa are 3.5, 1.1, and 2.4% , respectively. All of these chars were made previously in our laboratory, and details of their preparation were reported elsewhere.[32,33]

The reduction of NO by char was carried out for all chars at 5 – 6 temperatures between 723 and 1073K in a 10 mm ID VYCOR® glass vertical packed bed reactor with a fritted quartz disc of medium porosity as a support. For each run, 0.2 g char mixed with 2 g silicon carbide (inert materials for the reduction of NO) was packed in the reactor, and heated in He to the maximum temperature desired using an electric furnace. NO diluted with He (3130 ppm of NO) was then fed downward through the reactor for about 1 hour, when a pseudo-steady state was reached. Data were subsequently collected at 5 to 6 flow rate settings between 100 and 500 ml/min (NTP) at each of the temperatures studied. For each run, it took about 4 hours to collect all the data, and the burnout of the char was about 10% during that period of time. The inlet gas pressure in the reactor was controlled at 300 kPa (3 atm). The outlet pressure at each condition was also measured to determine the pressure drop cross the packed bed.

The compositions of outlet gases were continuously monitored for N_2 , CO, CO_2, N_2O, and O_2 by a GC (Perkin-Elmer, 3920B) with TCD and two columns (one packed with Chromosorb 106, the other packed with molecular sieve 5A), and for NO and NO_2 by a Chemiluminescence NO_x analyzer (Thermo Environmental, 42H). The variations in nitrogen and oxygen mass balances were determined between inlet and outlet streams for each run and always fell within ±5%.

RESULTS AND DISCUSSION

Pretests and Corrections. A typical plot of NO conversion vs. time shows that decreases from 100% to its pseudo-steady state value after about 1 hour. This probably results from NO adsorption on the sample and/or very active char surface sites that are quickly consumed. Thereafter, the conversion of NO decreases very slowly because of the loss of char mass. In order to account for the effect of the char mass loss in the calculation of kinetic parameters, a correction was made based on a carbon mass balance using the following stoichiometric reaction:

$$C + (1+y)\,NO = (1-y)\,CO + y\,CO_2 + 1/2(1+y)\,N_2 \qquad (1)$$

where $y = [CO_2]/([CO]+[CO_2])$, and [CO] and $[CO_2]$ are concentrations of CO and CO_2, respectively. Since [CO] and $[CO_2]$ are measurable quantities, the mass loss of char, ML (g), can be calculated

$$ML = 12 \cdot t \cdot F^0_{NO} \cdot X_{NO}/(1+y) \qquad (2)$$

where t is reaction time elapsed (min); X_{NO} is average conversion of NO in this period; F^0_{NO} is the inlet molar flow rate of NO (mol/min) calculated from the ideal gas law.

Figure 1 shows the variation of char mass (W) with the NO conversion (X_{NO}) in the form of the integrated rate expression, where the char mass has been corrected using Eq. 2, for the beginning and end of run. Since both sets of values fit the same straight line, the effect of the char mass loss on the reaction rate constant has been eliminated.

As mentioned, the inlet reactor pressures was typically 3.0 atm., but the outlet pressures varied with flow rate. In the calculation of concentration used in the kinetic rate expression, an average pressure $P = (P_{in} + P_{out})/2$ was used. Figure 2 shows how using this approach gives kinetic data that all fell on the same straight line for runs in which the pressure was varied (P_{in} from 1.5 to 3.0 atm. and P_{out} from 1.2 to 2.8 atm.) and the total flow rate was varied.

The calculation of film mass transfer and pore diffusion resistances for a worst case scenario (the maximum particle diameter, the minimum flow rate, and the maximum reaction rate observed) indicated that film mass transfer (maximum MT resistance = 2.7%) and pore diffusion (minimum effectiveness factor = 0.99)were negligible in this study.

Kinetics. Because a broad range of NO conversion was observed in this study, the reactor was modeled as an integral plug flow reactor. The reaction rate constants and reaction order were obtained by integral analysis of the experimental data. Briefly, the differential form of the plug flow reactor performance equation is

$$dW/F^0_{NO} = dX_{NO}/ -r_{NO} \qquad (3)$$

If the reaction is first order in NO (as confirmed later), integrating Eq. (3) produces the integrated rate expression as

$$-\ln (1-X_{NO}) = k_1\, C^0_{NO}\, W/F^0_{NO} \qquad (4)$$

where X_{NO} = NO conversion (= (moles NO in - moles NO out) / moles NO in); F^0_{NO} = inlet molar flow rate of NO (moles/s); W = char weight (g); $-r_{NO}$ = NO depletion rate (moles NO reacted/s*g_char); C^0_{NO} = initial NO concentration (moles/L); k_1 = first order rate constant (L/s*g_char).

Thus, if experimental data are plotted as $-\ln(1-X_{NO})$ vs. $C^0_{NO}\, W/F^0_{NO}$ and a straight line is obtained that passes through the origin, then evidence of 1st order kinetics is obtained and the slope of the line equals the value of the rate constant, k_1.

The experimental data for NDL char plotted as $-\ln(1-X_{NO})$ vs. $C^0_{NO}\, W/F^0_{NO}$ are shown in Figure 3, indicating that the reaction is first order with respect to NO. Attempts to fit the data to other orders were made, but straight lines were not obtained for all temperatures. Table 1 lists values for the reaction rate constants, their lower and upper 95% confidence limits, and statistical analysis parameters for NDL char data obtained at 6 different temperatures. The correlation coefficients, t-test values, and F-test values all show that the experimental data were excellently fit by first order kinetics under the experimental conditions. The standard error was typically less than 5%. Similar results were obtained for the other two chars, NDW and NCa.

The Effect of CaO. The variations of NO conversion with temperature are shown in Table 2 for three char types at a flow rate of 303 ml/min (NTP) . The results for other flow rates are similar. The conversion of NO increases noticeably in the order NDL > NCa > NDW. This is in the same order as the CaO content of the three chars, 3.5% > 2.4% > 1.1%. Therefore, the effects of CaO on the reaction of NO with chars appear to be significant.

Figure 4 shows the Arrhenius plots of the rate data for NDL, NDW, and NCa chars. The bars around points in the figure show the variation of the reaction rate constants in 95% confidence level. A sharp shift in the apparent activation energy with temperatures was observed, as also reported in literature.[6,7,15-18] The temperatures at which the transition takes place are in the range of 823 ~973 K, and decrease as the CaO content increases. This shift to higher activation energy with increasing temperature is opposite to the expectation if a reaction is changing from chemical rate control to mass transfer control, and suggests different mechanisms or rate determining steps at high and low temperatures. It is also noted that at low temperatures the apparent activation energies for all three char types are essentially the same (22 ~ 26 kcal/mol); at high temperatures, however, the activation energies vary from 45 to 60 kcal/mol, increasing as the CaO content of the

chars decreases. The variation of the NO reduction reactivity, the apparent activation energy, and the transition temperature with the CaO content are summarized in Table 2.

Discussion. The active surface sites of carbon are generally classified as edge sites and basal sites. At low temperatures, the reactivity of the basal sites can be negligible, compared to that of the edge sites.[21] In addition to the active sites of carbon, there exist other active sites, including sites on the surface of CaO, K_2O, CuO, and other potential catalysts. These active sites, as chemical or structural impurities, enhance the carbon edge sites; they can also chemisorb NO dissociatively like the carbon active sites. While chemisorbed oxygen migrates to and reacts with the carbon edge sites around, the chemisorption of NO on the inorganic sites continues. Therefore, CaO, K_2O, CuO *etc.* may exhibit catalytic effects on the reaction of NO with char.

The reactivity of NO with char increases significantly with increasing CaO content. Such increase involves two aspects. On one hand, an increase in CaO content provides more defects of coal structure, the reactivity of char then increases; on the other hand, the catalytic effects of CaO also increase due to more active CaO sites. The reaction of NO with char may not proceed as a simple catalytic process. Two routes may exist in parallel, which are the direct reduction of NO on active carbon sites and the catalytic reduction of NO through active CaO sites. When there are enough active CaO available, the catalytic reduction route is predominant. On the other hand, when very few active CaO sites exist, the direct reduction route becomes predominant. Between the two extreme cases, which most actual cases may belong to, the reduction of NO may be controlled by the both routes. Therefore, the two parallel processes should be taken into account in the mechanism of the reaction of NO with char. A possible parallel reaction model may be described as follows:

$$NO + 2C^* \rightarrow C^*(O) + C^*(N) \quad (1a)$$
$$NO + 2C \leftrightarrow C(O) + C(N) \quad (1b)$$
$$NO + 2S \rightarrow S(O) + S(N) \quad (1c)$$
$$2C^*(N) \text{ (or } S(N)) \rightarrow N_2 + 2C^* \text{(or } S) \quad (2)$$
$$S(O) + C^* \rightarrow C^*(O) + S \quad (3a)$$
$$C(O) + C^* \rightarrow C^*(O) + C \quad (3b)$$
$$C^* + C^*(O) + NO \rightarrow CO_2 + C^*(N) \quad (4)$$
$$C^*(O) \rightarrow CO \quad (5)$$
$$C^*(O) + CO \rightarrow CO_2 + C^* \quad (6)$$
$$2C^*(O) \rightarrow CO_2 + C^* \quad (7)$$
$$CO_2 + C^* \rightarrow 2C^*(O) \quad (8)$$

where C^* is the carbon edge sites; C is the basal sites; S is the active sites of catalysts. Reactions 1a, 1b, 1c are parallel processes of the dissociative chemisorption of NO. The desorption of the chemisorbed oxygen involves only the carbon edge sites (C^*) represented by Reaction 4, 5, 7, and 8, which are parallel routes. All oxygen atoms adsorbed on the other active sites (C or S) need to migrate to the carbon edge sites before desorption as described by Reaction 3a, 3b. On the bases of the facts of the delay in CO_2 or CO evolution with respect to N_2 [27-29] and the positive effects of O_2 on the reaction of NO with char,[5] it is reasonable to assume that the desorption of the chemisorbed oxygen is the rate determining steps. At low temperatures, Reactions 5 and 8 may be slow; therefore, the reaction rate of NO with char may depend on Reactions 4, 6, 7 or a combination of these reactions, and CO_2 is a dominant product of C-containing species; at high temperatures, however, Reactions 5 and 8 become fast, and Reaction 5 will be a major pathway of the desorption of the chemisorbed oxygen, so that Reaction 5 controls the reaction rate of NO with char, and CO becomes a dominant product. With the shift in the rate determining step, the apparent activation energy also changes as shown in Figure 4.

Since the reduction of NO by char is composed of two parallel processes, i.e. the direct reduction of NO on active carbon sites and the catalytic reduction of NO through active CaO sites, it seems that the apparent activation energy for the global reaction of NO with char is a combination of the activation energies of the two parallel processes in some way. When the CaO content (actually the CaO surface area) increases, the proportion of the catalytic reduction may increase. If the activation energy for the catalytic reduction is lower than that for direct reduction (a reasonable assumption), the apparent activation energy will decrease as the CaO content increases as listed in Table 2 for the high temperature data.

CONCLUSION

The kinetics of the reaction of NO with char have been determined for three kinds of chars with different CaO contents. The reaction is first order with respect to NO partial pressure, and has a sharp shift in the activation energy with temperature. The shift temperature decreases as the CaO content in the chars increases. At low temperatures, the activation energies for all three char types are essentially the same (22-26 kcal/mol); at high temperatures, however, the activation energies vary in the range of 45 to 60 kcal/mol, and increase as the CaO content decreases. The migration of the chemisorbed oxygen on basal carbon sites to carbon edge sites at high temperatures may result in a shift in the rate determining step, so that a shift in the activation energy takes place . When the CaO content increases, the activation energy of the migration of the chemisorbed oxygen may decrease; hence, the shift temperature decreases.

Acknowledgments. This work was sponsored by the Advanced Combustion Engineering Research Center at Brigham Young University. Funds for this center are received from the National Science Foundation, the State of Utah, the U. S. Department of Energy, and a number of industrial participants. We also thank Richard F. Cope for char preparation and Troy Ness for technical assistance.

References

(1) Bosch, H. *Catalysis Today*, **1988**, 2, 1.
(2) Pereira, F. J.; Beer, J. M.; Gibbs, B.; Hedley, A. B. *15th Symposium (International) on Combustion*; The Combustion Institute: Pittsburgh, 1975, p1149.
(3) Johnson, J. E. *Fuels* **1994**, 73, 1398.
(4) Illan-Gomez, M. J.; Linares-Solano, A.; Salinas-Martinez de Lecea, C. *Energy Fuels* **1993**, 7, 146.
(5) Yamashita, H.; Tomita, A., *Energy Fuels* **1993**, 7, 85.
(6) Teng, H.; Suuberg, E. M.; Calo, J. M. *Energy Fuels* **1992**, 6, 398.
(7) Furusawa, T.; Tsunoda, M.; Tsujimura, M.; Adschiri, T. *Fuel* **1985**, 64, 1306.
(8) Furusawa, T.; Kunii, D.; Osuma, A.; Yamada, N. *Int. Chem. Eng.* **1980**, 20, 239.
(9) Wendt, J. O. L.; Pershing, D. W.; Lee, J. W.; Glass, J. W. *17th Symposium (International) on Combustion*; The Combustion Institute: Pittsburgh, 1979, p77.
(10) Levy, J.; Chan, L. K.; Sarofim, A. F.; Beer, J. M. *18th Symposium (International) on Combustion*; The Combustion Institute: Pittsburgh, 1981, p111.
(11) Watts, H. *Trans. Faraday Soc.* **1958**, 54, 93.
(12) Smith, R. N.; Swinehart, J.; Lesnini, D. *J. Phys. Chem.* **1959**, 63, 544.
(13) Richthofen, A. V.; Wendel, E.; Neuschiitz, D. *Fresenius' J. Anal. Chem.* **1993**, 346, 261
(14) Edwards, H. W. *AIChE Symp. Ser. No. 126*, **1972**, 68, 91.
(15) Song, Y. H.; Beer, J. M.; Sarofim, A. F. *Combust. Sic. Technol.* **1981**, 25, 237.
(16) Chan, L. K.; Sarofim, A. F.; Beer, J. M. *Combust. Flame* **1983**, 52, 37.
(17) Radovic, L. R.; Walker, Jr., P. L. *Fuel Process Technol.* **1984**, 8, 149.
(18) Suuberg, E. M.; Teng, H.; Calo, J. M. *23rd Symposium (International) on Combustion*; The Combustion Institute: Pittsburgh, 1990; p1199.
(19) Teng, H.; Suuberg, E. M. *J. Phys. Chem.* **1993**, 97, 478.
(20) Teng, H.; Suuberg, E. M. *ind. Eng. Chem. Res.* **1993**, 32, 416.
(21) Chu, X., Schmidt, L. D. *Ind. Eng. Chem. Res.* **1993**, 32, 1359.
(22) Lai, C.-K. S.; Peters, W. A.; Longwell, J. P. *Energy Fuels* **1988**, 2, 586.
(23) Matos, M. A. A.; Pereira, F. J. M. A.; Ventura, J. M. P. *Fuel* **1991**, 70, 38.
(24) Shimizu, T.; Sazawa, Y.; Adschiri, T.; Furusawa, T., *Fuel* **1992**, 71, 361.
(25) Yamashita, H.; Yamada, H.; Tomita, A. *Applied Catalysis*, **1991**, 78, L1-L6.
(26) Furusawa, T; Koyama, M; Tsjimura, M. *Fuels* **1985**, 64, 413.
(27) Illan-Gomez, M. J.; Linares-Solano, A.; Radovic, L.; Salinas-Martinez de Lecea, C. *Energy Fuels* **1995**, 9, 97.
(28) Illan-Gomez, M. J.; Linares-Solano, A.; Radovic, L.; Salinas-Martinez de Lecea, C. *Energy Fuels* **1995**, 9, 104.
(29) Illan-Gomez, M. J.; Linares-Solano, A.; Radovic, L.; Salinas-Martinez de Lecea, C. *Energy Fuels* **1995**, 9, 112.
(30) Johnson, J. E.; Dam-Johansen, K. *11th International Conference on Fluidized Bed Combustion*, American Soc. Mech. Eng., New York, 1991, p1389.
(31) De Soete, G. C. *23rd Symposium (International) on Combustion*; The Combustion Institute: Pittsburgh, 1990; p1257.
(32) Cope, R. F.; Arrington, C. B.; Hecker, W. C. *Energy fuels* **1994**, 8, 1059.
(33) Cope, R. F. *Dissertation*, Brigham Young University, Provo, Utah, 1995.
(34) Illan-Gomez, M. J.; Linares-Solano, A.; Radovic, L.; Salinas-Martinez de Lecea, C. 8th International conference on Coal Science, Oviedo, Spain, 1995, p1911.

Table 1 The Reaction Rate Constants of NDL Char and Statistical Analysis

T	k_1	k_1	k_1	Std Error	Corr Coef	t Test	t-distrib	F Test	F-distrib
°C	L/sec*g_char	Low 95%	Up 95%		r^2		α=0.01		α=0.01
650	0.0736	0.0562	0.0909	4.03E-03	0.994	18.2	9.925	333	199
625	0.0353	0.0333	0.0373	7.29E-04	0.998	48.5	4.604	2348	26
600	0.0182	0.0161	0.0202	7.40E-04	0.993	24.6	4.604	457	26
600	0.0181	0.0158	0.0205	8.48E-04	0.991	21.4	4.604	604	26
550	0.0070	0.0063	0.0078	2.66E-04	0.994	26.5	4.604	701	26
500	0.0029	0.0026	0.0032	1.10E-04	0.994	26.2	4.604	686	26
470	0.0016	0.0016	0.0017	2.56E-05	0.999	64.1	4.604	4103	26

Table 2 NO Reduction Reactivity, Apparent Activation Energy and Transition Temperature for Three Char types

	CaO	T @50% conv.	Transition T	App. Act. Energy (kcal/mol)	
	%	(Q=303ml/m), K	K	High Temp	Low Temp
NDL	3.5	875	853	44.5±5	22.2±3
NCa	2.4	940	893	53.1±5	26.2±3
NDW	1.1	980	953	59.5±5	22.7±3

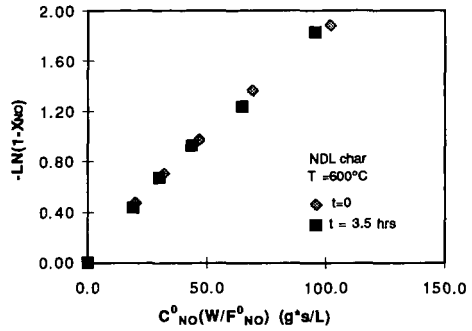

Figure 1 The effect of run time on the integrated rate expression after the char mass loss correction.

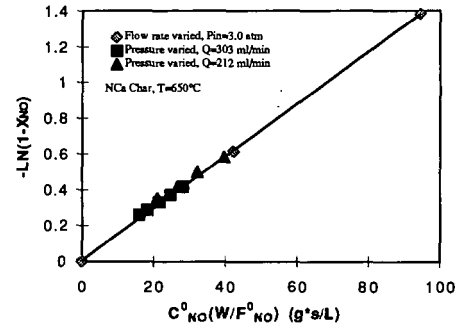

Figure 2 The effect of pressure and flow rate (P_{out}) on the integrated rate expression, using $P_{bed} = 1/2(P_{in} + P_{out})$.

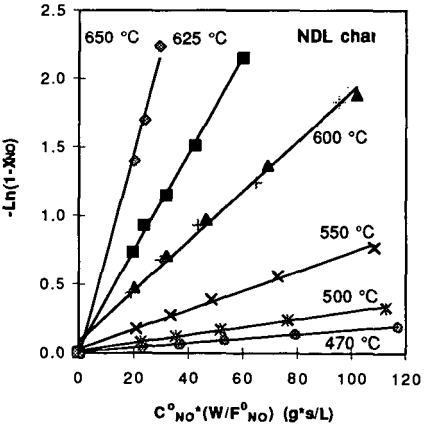

Figure 3 Experimental data for NDL char plotted as $-\ln(1-X_{NO})$ vs. $C^{o}_{NO}W/F^{o}_{NO}$

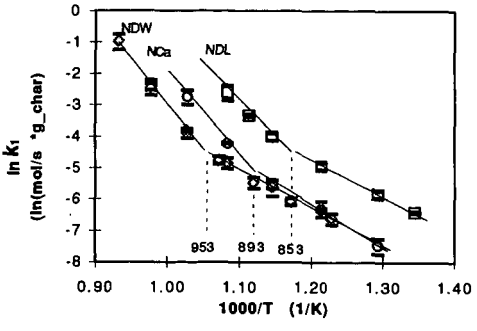

Figure 4 Arrhenius plots of the reaction rate constants for NO reduction with char for three chars.

NO_x AND SO_2 ADSORPTION ON CARBON

Aurora M. Rubel and John M. Stencel
Center for Applied Energy Research
University of Kentucky
Lexington, KY 40511-8433, USA

Keywords: NO_x, SO_2, adsorption, carbon

INTRODUCTION

The need to control NO_x emissions from fossil fuel power plants has lead to the development of commercially proven technologies, the best known being selective catalytic reduction (SCR)[1-3]. Because NO_x concentrations are generally at near trace levels and less than 0.3%[4], a number of other potentially more efficient control measures have and are being investigated. One such measure includes the use of adsorbents such as metal oxides[5,6], ion-exchanged zeolites[7], activated carbon fibers with and without modifiers[8-10], and activated carbons[11-15].

Activated carbons can be used effectively for SCR and for the oxidation of SO_2 to SO_3 with the subsequent formation of H_2SO_4[16-19]. The uptake of SO_2 by carbons in the absence of NO_x has been studied extensively[20-26]. Moisture[20-22], O_2 content[22-25], and temperature[24] influence greatly the amount of SO_2 adsorbed onto activated carbons, although agreement is lacking on the synergistic or detrimental effects of co-adsorbed O_2 and H_2O[22-25]. It has been suggested that two different sites on the carbon are involved in SO_2 adsorption and oxidation[26], and that two different SO_2 species are present on the carbon during and after adsorption[22-25].

NO adsorption onto activated carbons over a temperature range of 20-120°C and in the absence of SO_2 have been reported[11-15, 27-29]. Without O_2, a carbon's NO uptake capacities and adsorption kinetics were low[27, 28] in comparison to when O_2 was present as a co-adsorbate[11-13]. These data have shown that the adsorption of NO from a simulated flue gas containing O_2, CO_2, and H_2O involved the catalytic conversion of $NO + \frac{1}{2} O_2 \rightarrow NO_2$ at active site(s) on the carbon[11-13] leading to NO_x adsorption capacities as high as 200 mg NO_2 (g carbon)$^{-1}$. No published work has been found which details adsorption capacities and kinetics during the co-adsorption of NO and SO_2 over activated carbons or other porous materials. However, an understanding of the effects of such co-adsorption is very important because the combustion flue gas from every type of fossil fuel will contain SO_2 and NO_x. Hence, this work was performed to elucidate interactions between NO_x and SO_2 in and over activated carbons during adsorption and desorption cycling.

EXPERIMENTAL

Instrumentation. NO_x/SO_2 adsorption/desorption profiles were obtained using a Seiko TG/DTA 320 coupled to a VG Micromass PC quadrupole mass spectrometer (MS). A heated (170°C) fused silica capillary was used to transfer an aliquot of the atmosphere above the sample pan in the thermogravimetric analyzer (TG) to an inert metrasil molecular leak which interfaced the capillary with the enclosed ion source of the MS. Both instruments were controlled by computers which also provided for programmable control of the furnace, continuous weight measurements, sweep gas valve switching, data acquisition and analysis, review of MS scans and export of data to other computers. The MS has a Nier type enclosed ion source, a triple mass filter, and two detectors (a Faraday cup and a secondary emissions multiplier).

TG-MS procedures. The TG sample pan was loaded with a constant activated carbon volume weighing approximately 20-30 mg. The sweep gas flow rate through the TG was held constant at 200 ml m^{-1} metered at room temperature and pressure. The heating regime of the furnace incorporated segments in the following order for pre-conditioning, cooling, adsorption, reversible desorption, and temperature-induced (irreversible) desorption. Explanations of each step and example programs have been previously published[11,13]. For this study, the pre-conditioning and irreversible desorption heating rate, adsorption time interval, reversible desorption time, and the maximum desorption temperature were 20 °C m^{-1}, 60 m, 30 m, and 350 ° C respectively. A He gas sweep was used during pre-conditioning, and reversible and irreversible desorptions. Pre-conditioned carbon was exposed to simulated flue gas only during the adsorption step. Multiple and consecutive adsorption/desorption cycles could be performed by recycling the furnace temperature program.

The MS was used to continuously monitor gases during an experiment. Spectral scans were acquired over a 1-100 a.m.u. range with a total measurement interval of approximately 30 s per 100 a.m.u..

Mass ion identification, analytical procedures, and materials. The identification of desorbed gases detected by the MS was done by using the major mass ions, 64, 44, 32, and 18, for SO_2, CO_2, O_2, and

H_2O respectively. The major mass ion for both NO and NO_2 is 30. The relative abundance of a.m.u. 46 for NO_2 gas is approximately 40 percent, but in mixtures of gases, this value can change. Therefore, NO and NO_2 were identified by comparing the mass ion ratio, 30/46, during desorption with ratios determined using mixtures of NO or NO_2 and all combinations of gases used during our study.

A carbon, commercially produced by physical activation with steam, was used. The carbon had N_2 BET total, meso- and micropore surface areas and pore volumes of 460, 20, and 440 $m^2\ g^{-1}$ and 0.69, 0.45, and 0.24 ml g^{-1} respectively. The chemical and physical properties of this carbon, identified as carbon, **a**, in a previous publication, has been described in detail[15]. Carbon pre-conditioned under a flow of He or SO_2 was used.

Three simulated flue gas mixtures were used during this study. The concentrations of O_2, CO_2, and H_2O were held constant at 5%, 15%, and 0.4-0.6% respectively. The NO and SO_2 composition of the three mixtures were varied as follows: 1% NO with 0% SO_2, 1% NO with 0.025% SO_2, and 0% NO with 0.025% SO_2. He was used as the balance gas. The primary variable studied was the simulated flue gas composition at an adsorption temperature of 70°C.

RESULTS AND DISCUSSION

Adsorption/desorption profiles shown in Figure 1 were generated during each TG/MS experiment. The weight gained, weight lost and an identification of the desorbed gas species were determined using these profiles. Figure 1 shows a profile for the co-adsorption of NO_2 and SO_2 at 70°C. Carbon pre-conditioning is performed up to point **a**. The weight gained upon exposure of the carbon to the simulated flue gas (points **a**-to-**b**) was attributed to the adsorption of gas components. Weight lost at the adsorption temperature after switching from the simulated flue gas to He (points **b**-to-**c**) was attributed to "reversibly adsorbed" species. Weight lost as a consequence of increasing the temperature of the carbon (points **c**-to-**d**, and beyond), i.e. during temperature programmed desorption (TPD), was attributed to two "irreversibly adsorbed" species which evolved at different temperatures. They were identified by MS as NO_2 and SO_2 and were the only evolved gas species detected. Upon reaching the maximum desorption temperature, the carbon weight returned to the pre-adsorption starting weight.

Weight gain curves during exposure of the activated carbon to the three different flue gas mixtures are presented in Figure 2. The total uptake decreased from 143 mg (g carbon)$^{-1}$ -to- 129 mg (g carbon)$^{-1}$ when SO_2 was a constituent in the gas. Pre-saturating the carbon with SO_2 prior to exposure to gases containing both NO and SO_2 decreased further the total uptake to 109 mg (g carbon)$^{-1}$. In the presence of SO_2 only (no NO), the uptake was only 24 mg (g carbon)$^{-1}$.

The desorption weight loss curves, presented in Figure 3, were defined with respect to reversible and irreversible (TPD) components. Reversible desorption accounted for 18%, 36% and 58% of the total uptake for gases containing both NO and SO_2, NO alone, or SO_2 alone, respectively. Figure 4 shows the DTG curves acquired during TPD and Figure 5 gives the desorption weights which could be attributed to specific evolved gases by MS. For simulated flue gas containing NO and SO_2, two irreversibly adsorbed species desorbed from the carbon and were identified to be NO_2 and SO_2. The temperature of maximum evolution was 145°C for NO_2 and 319°C for SO_2 (also see Figure 1). The adsorption of NO_2 in the absence of SO_2 also gave two irreversibly adsorbed species, having temperatures of maximum evolution at 144°C and 352°C. These two irreversible components were identified as NO_2 and CO_2, respectively. Only one irreversibly adsorbed species, identified as SO_2, was desorbed from the carbon after exposure to gas containing SO_2 (no NO). The maximum evolution of this SO_2 occurred at 302°C.

When SO_2 was present, the amount of irreversibly adsorbed NO_2 decreased to 68 mg (g carbon)$^{-1}$ from 87 mg(g carbon)$^{-1}$ when SO_2 was not present (Figure 5). The amount of irreversible NO_2 species further decreased to 59 mg (g carbon)$^{-1}$ when the carbon was pre-saturated with SO_2. However, the amount of irreversibly bound SO_2 was doubled when SO_2 was adsorbed in the presence of NO in comparison to when SO_2 was adsorbed by itself. This enhancement suggests that there is synergistic interaction between NO_2 and SO_2 during adsorption onto the carbon. Another observation was the fact that carbon pre-saturated with SO_2 and then exposed to the NO + SO_2 - containing flue gas (compare Figures 2 and 5) adsorbed more SO_2 than without the pre-saturation. Additionally, the temperature of desorption for the irreversibly adsorbed SO_2 species was increased from 300°C (in the case of SO_2 adsorption without NO) to 320°C when SO_2 and NO_2 are co-desorbed.

We have previously postulated that NO_2 adsorption involved the catalytic conversion of NO + ½ O_2 → NO_2 at an active site(s) on the carbon and that NO_2 then condenses within the micropores of the carbon[13]. It is possible that active sites are created during the co-adsorption of NO_2 and SO_2 that are

not created during the adsorption of SO_2 by itself, or the presence of NO_2 on the surface may assist the oxidation of $SO_2 \rightarrow SO_3$ on the carbon which enhanced the uptake of SO_2. Relative to the effects of SO_2 on the uptake capacity of NO_2 , it may bind to or interfere with the sites involved in the catalytic conversion of NO-to-NO_2, thereby resulting in lower NO_2 adsorption.

The temperature of maximum evolution of NO_2 was not altered by the presence of SO_2, indicating that the mechanism of condensation of NO_2 within the micropores was not affected by SO_2 surface species. Because condensation of NO_2 within the micropores would be strongly dependent on van der Waal forces[5,10,12], and because SO_2 and NO_2 have similar van der Waal force constants, it is possible that adsorbed SO_2 would not affect the NO_2 storage mechanism. However, SO_2 has a critical volume 1.5 times that of NO_2 and has stronger bonding to the carbon. Both of these factors would suggest that the adsorbed SO_2 species may concentrate at pore mouths, a location which would limit NO_2 condensation. The slower rate of reversible desorption when $NO_2 + SO_2$ are co-adsorbed (Figure 3) in comparison to adsorption of NO_2 alone may also reflect a physical impediment related to SO_2; for instance SO_2 bound to active sites could limit or block the access of NO_2 to the micropores, thereby affecting not only the storage capacity but also the rate of adsorption/desorption.

In fact, the maximum adsorption rate and the desorption rate for the irreversibly adsorbed NO_2 species were decreased by the co-adsorption of SO_2 (Figure 6). Good correlations ($r^2 = 1.00$) were obtained for the decline in the maximum adsorption rate (second order) and desorption rate (first order) versus the amount of SO_2 adsorbed. We have previously reported that the NO_2 adsorption capacity of different carbons was dependent on the maximum adsorption rate of NO_2, but that the desorption rate of the irreversibly adsorbed NO_2 species was the same for all carbons[15]. For the current study, the amount of NO_2 stored in the carbon versus the maximum adsorption rate, as influenced by SO_2, resulted in a good second order correlation, $r^2 = 0.995$ (Figure 7).

SUMMARY AND CONCLUSION

During the co-adsorption of NO_2 and SO_2 from a simulated flue gas, less NO_2 and substantially more SO_2 was adsorbed in comparison to when either oxide was adsorbed by itself. The adsorption mechanism for NO_2 remained unchanged in the presence or absence of SO_2. When NO_2 and SO_2 were co-adsorbed, a synergism improved the capacity of the carbon for SO_2 uptake. The presence of adsorbed SO_2 in the carbon significantly decreased the rate of adsorption and the rates of both reversible and irreversible desorption of NO_2, indicating the possibility of a physical impediment created by the adsorbed SO_2.

REFERENCES

1. Bosch, H. and Janssen, F. *Catal. Today* 1988, **2**, 369
2. Grzybek, T. and Papp, H. *Appl. Catal. B. Environ.* 1992, **1**, 271
3. Radtke, F., Koeppel, R.A., and Baiker, A. *Appl. Catal.* A 1994, **107**, L125
4. Ritter, J.A. and Yang, R.T. *Ind. Eng. Chem. Res.* 1990, **29**, 1023
5. Arai H. and Machida M., *Catalysis Today* 1994, **22**, 97
6. Stiles, A. B., Klein, M.T., Gauthier, P., Schwarz, S., and Wang, J. *Ind. Eng. Chem. Res.* 1994 **33**, 2260
7. Zhang, W.,Yahiro,H., Mizuno, N., Izumi, J., and Iwamoto, M., *Langmuir* 1993, **9**, 2337
8. Kaneko, K., Shindo, N. Carbon 1989, **27**, 815
9. Knoblauch, K., Richter, E. and Juntgen, H. *Fuel* 1981, **60**, 832
10. Kaneko, K., Nakahigashi, Y. and Nagata, K. *Carbon* 1988, **26**, 327
11. Rubel, A.M., Stencel, J.M., and Ahmed, S.N. *Preprints Symposium on Flue Gas Cleanup Processes* 1993, ACS, Division of Fuel Chem., Denver, CO meeting, 726.
12. Rubel, A.M., Stencel, J.M., and Ahmed, S.N. *Proceeding of the AIChE 1993 Summer National Meeting* 1993, Seattle, WA,, paper no. 77b.
13. Rubel, A.M., Stewart, M.L. and Stencel, J.M. *JMR* 1994, **10**, 562.
14. Rubel, A.M. and Stencel, J.M. *Energy and Fuel*, in press
15. Rubel, A.M., Stewart M.L., and Stencel, J.M. In *Reduction of Nitrogen Oxide Emissions, ACS Symposium Series 587*, Ozkan, U.S., Agarwal, S.K., and Marcelin, G. eds., ACS, Washington, D.C. 1995,208
16. Cha, C.Y. *Res. Chem. Imtermed.* 1994, **20**, 13
17. Gangwal, S.K., Howe, G.B., Spivey, J.J., Silveston, P.L., Hudgins, R.R., and Metzinger, J.G. *Environ. Prog.* 1993, **12**, 128
18. Ahmed, S.N., Stencel, J.M., Derbyshire, F.J., Baldwin, R.M. *Fuel Proc. Tech.* 1993, **34**, 123
19. Ahmed, S.N., Baldwin, R.M., Derbyshire, F.J., McEnaney, B., and Stencel, J.M. *Fuel* 1993, **72**, 287
20. Zawadzki, J. *Carbon* 1987, **25**, 43
21. Zawadzki, J. *Carbon* 1987, **25**, 495
22. Tartarelli, R., Davini, P., Morelli, F., and Corsi, P. *Atmosph. Environ.* 1978, **12**, 289

23. Davini, P. *Carbon* 1991, **28**, 565
24. Davini, P. *Carbon* 1991, **29**, 321
25. Carrasco-Marin, F., Uterra-Hidalgo, E., Rivera-Utrilla, J., Moreno-Castilla, C. *Fuel*, 1992, **71**, 575
26. Mochida, I., Hirayama, T., Kisamori, S., Kawano, S., and Fujitsu, H. *Langmuir* 1992, **8**, 2290
27. Teng, H. And Suuberg, E.M. *J. Phys. Chem.* 1993, **97**,478
28. DeGroot, W.F., T.H. Osterheld, G.N. Richards. *Carbon* 1991, **29**,185
29. Richter, E., R. Kleinschmidt, E. Pilarczyk, K. Knoblauch, and H. Juntgen. *Thermochimica Acta* 1985, **85**,311

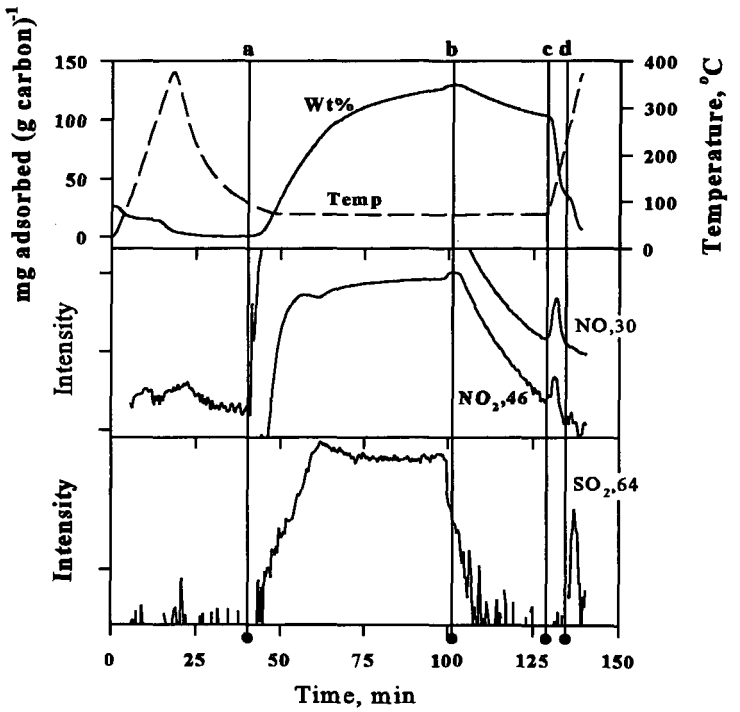

Figure 1. Adsorption-desorption profile from TG-MS for adsorption of NO_2 and SO_2 at 70°C.

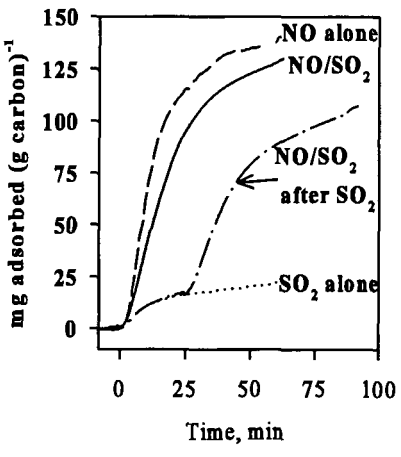

Figure 2. Weight gain curves during adsorption.

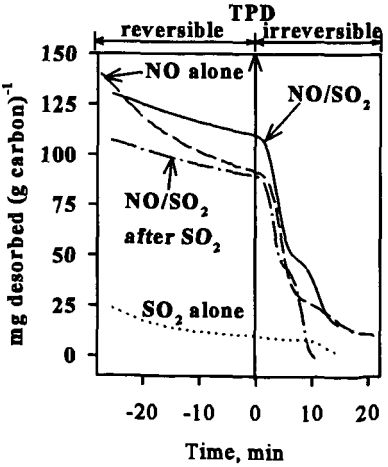

Figure 3. Weight loss curves during TPD.

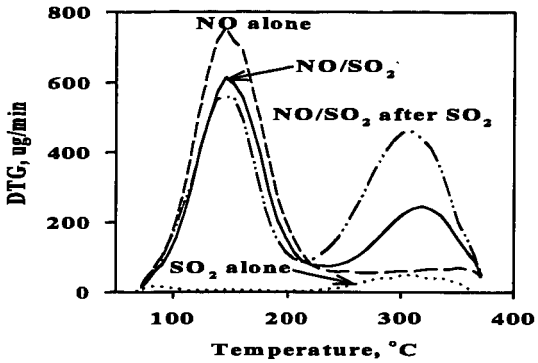

Figure 4. DTG curves during irreversible desorption.

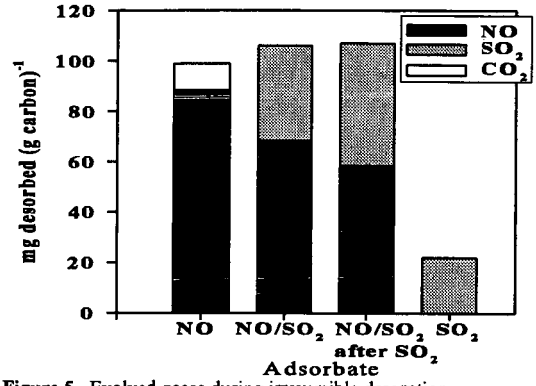

Figure 5. Evolved gases during irreversible desorption.

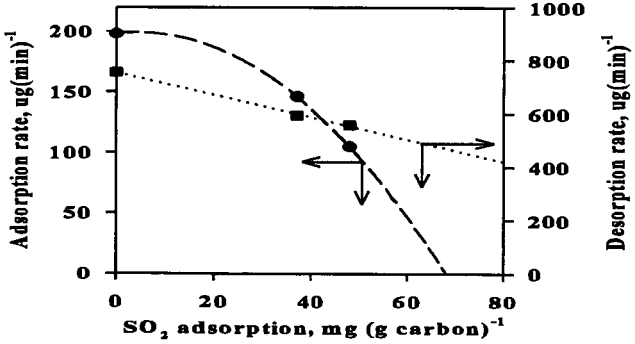

Figure 6. Influence of adsorbed SO_2 on adsorption and desorption rates.

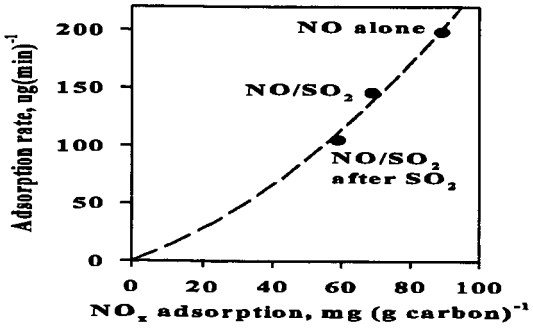

Figure 7. Correlation between NO_x adsorption capacity and total adsorption rate.

INTERACTION OF SO_x AND NO_x WITH SOOT

A. R. Chughtai, M. M. O. Atteya, B. K. Konowalchuk,
M. L. Rosenberger, and D. M. Smith
Department of Chemistry, University of Denver
Denver, CO 80208

Keywords: SO_x, NO_x, Soot

INTRODUCTION

As part of a continuing study of the heterogeneous reactions of black carbon with gas phase oxidant species, the adsorption of low concentrations (30 - 2000 ppm) of SO_2 and NO_2 individually, together, and in the presence of other adsorbates have been studied by spectroscopic and microgravimetric techniques. Previous work in this study has revealed a dual path mechanism for the reaction of NO_2/N_2O_4 with n-hexane soot over concentration range 9 ppm - 200 torr (1,2). (This soot has been used throughout these investigations as a model for fossil fuel-produced black carbon). The effect of simulated solar radiation on the reaction at lower pressures (9-35ppm) is in the diminution of the NO_2 reactant through its photolytic dissociation (2). An FT-IR study of the reaction of various nitrogen oxides with black carbon showed the only reactive species at 298K to be NO_2, with NO and N_2O unreactive (3). A spectroscopic examination of the gaseous products of the soot-oxides of nitrogen-water vapor reaction has revealed the formation of CO, CO_2, and N_2O, along with NO, from a redox reaction between NO_2/N_2O_4 and the most reactive components of soot during the reaction's early stages (4). At higher temperatures and NO_2/N_2O_4 pressures, n-hexane soot undergoes chemisorption and two types of redox reaction depending upon the conditions (5). The major redox reaction, for which an intermediate $C-(NO_2)x$ complex has been identified, is precluded by prior chemisorption but, if initiated, results in brisk oxidation of the carbon to CO and CO_2 (5). Previous studies of black carbon-SO_2-H_2O-O_2 reaction systems in these laboratories include the effect of simulated solar radiation in the formation of surface sulfate (6) and the effect of metal oxides with carbon on sulfate formation (7). Interaction of SO_2 and carbon represent the most intensively studied of the heterogeneous systems containing carbon. An attempt to understand the molecular dynamics involved in the reactions of carbon in the presence of multiple reactants, such as SO_2 and NO_2, underlies the present work.

RESULTS AND DISCUSSION

SO_2 Adsorption

Because those reactions of SO_x and NO_x in the presence of and with black carbon which are of interest to us occur in air, all adsorption studies were carried out in the presence of zero air (compressed air with CO_2 and H_2O removed). This immediately raises the question of any role of O_2 in SO_2 adsorption, one addressed in our other paper in this symposium (8), involving competition for adsorption sites. That work demonstrates no such direct competition, or at least weaker adsorption of SO_2, the presence of SO_2 showing no effect on the corrected normalized integral of soot's EPR signal (8).

Microgravimetric experiments in which 10 mg n-hexane soot was exposed to 600-2000 ppm SO_2 show a depletive adsorption as illustrated in Figure 1. At 60 min., just prior to the purge with zero air, the surface coverages (θ) by SO_2 were calculated from soot mass increase, its specific surface area of 89±2 m^2/g, and a molecular area for SO_2 of 19.2 $Å^2$(9), for each replicate run. A plot of θ versus P_{SO2} shows a linear dependence, Figure 2, for which the relationship

$$\theta = (5.06 \pm 0.07) \times 10^{-5} P_{SO2} + (18.16 \pm 0.08) \times 10^{-2} \quad (1)$$

obtains. A linear relationship between θ and P is expected at low pressures for adsorption systems obeying the Langmuir isotherm (10)

$$\theta = kP/(1+kP) \quad (2)$$

The intercept in this case suggests a second mode of SO_2 adsorption which may be determined by some surface

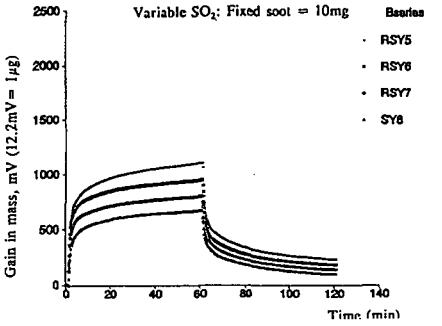

Figure 1. Adsorption of SO_2 on soot

characteristic. Independent evidence of another mode comes from Figure 1 in which the desorption of SO_2 by zero air asymptotically approaches a limiting mass reflecting retention of as much as 20% of the total adsorbed. A likely candidate for

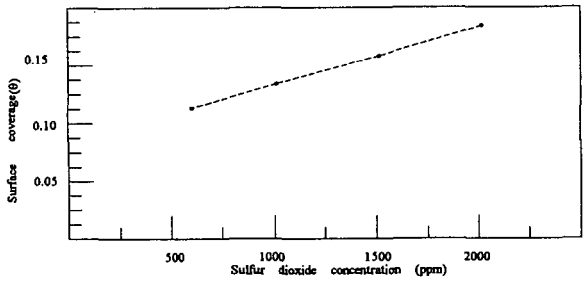

Figure 2. Plot of surface coverage (θ) as a function of P_{SO2}

this adsorption pathway is the surface hydrolysis of SO_2 to $SO_2.H_2O$ (H_2SO_3). The resulting reaction scheme

$$SO_2\ (g) + SS \underset{k_{-1}}{\overset{k_1}{\rightleftharpoons}} SS.\ SO_2\ (s) \quad (3)$$

$$SS.SO_2\ (s) + H_2O.ads \xrightarrow{k_2} SS.\ H_2SO_3\ (s) \quad (4)$$

where SS = surface site, could be followed by oxidation to sulfate

$$SS.H_2SO_3 + 1/2O_2 \xrightarrow{k_3} SS.\ H_2SO_4 \quad (5)$$

Small amounte of adsorbed water cannot be excluded from the soot surface under these conditions.

The effect of temperature on SO_2 adsorption was examined with a soot mass of 15 mg at 1010 ppm SO_2 by the same microgravimetric technique. Figure 3 shows a family of mass gain versus time curves over the temperature range 22°C to 66°C for the first 5

minutes of the adsorption experiment. These data represent surface coverages ranging from 8.6 to 2.2 percent, respectively, which exhibit a linear relationship to temperature. Utilizing microgravimetric data such as those of Figure 1, it is possible to estimate the fraction of adsorbed SO_2 which is irreversibly bound to the surface, as represented by equation 4,

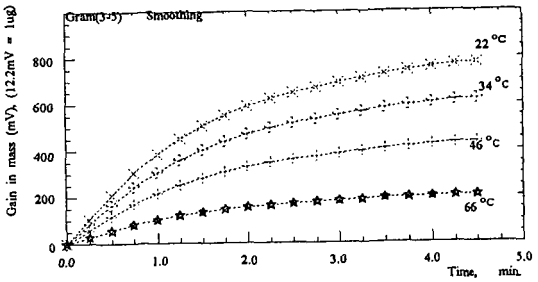

Figure 3. Mass gain versus time curves as a function of temperature.

at each temperature. From the total number of adsorbed molecules per gram, then, the reversibly adsorbed (physisorbed) SO_2 and a set of equilibrium constants for equation 3 have been calculated. These data are summarized in Table I.

Table I. Effect of Temperature on SO_2 Adsorption

Temperature, °C	SO_2 Surface Coverage, θ	Fraction of SO_2 physisorbed, f	$K_{eq} \times 10^{-16}$, molecules per g-ppm
22	0.0858	0.823	3.24
34	0.0684	0.810	2.54
46	0.0479	0.772	1.74
66	0.0225	0.763	0.79

Plots of $\log K_{eq}$ versus 1/T show some curvature reflecting the apparent fact that the enthalpy of physisorption for SO_2 on n-hexane soot is a function of surface coverage. Over the temperature range 22-66°C, this value averages 26.8 kJ/mol-K, a figure within the range of 20-27 kJ/mol found by Davini (11) for SO_2 adsorption on three oxidized carbons at 20°C and 1 atmosphere. By comparison, the molar heat of vaporization of SO_2 also is 26.8 kJ/mol at 22°C.

Coadsorption of SO_2 and NO_2

Spectroscopic and microgravimetric data from the NO_2/N_2O_4-soot system (1,2) over a wide concentration range conform to the Elovich equation, an isotherm for activated adsorption or chemisorption. The principal products at low concentration of NO_2 at laboratory temperatures are such functional groups as $-NO_2$, $-ONO$, $-NNO_2$. As noted above, on the other hand, SO_2 adsorption is primarily reversible, involves a low heat of adsorption and is more properly termed physisorption; however, up to 20% appears to be surface reactive or undergoes some type of chemisorption. Of interest in this work have been the molecular mechanisms of coadsorption of SO_2 and NO_2, given the different natures of their adsorption.

Figure 4 is a composite of microgravimetric curves of soot which summarizes its behavior during a series of SO_2 and NO_2 exposures.

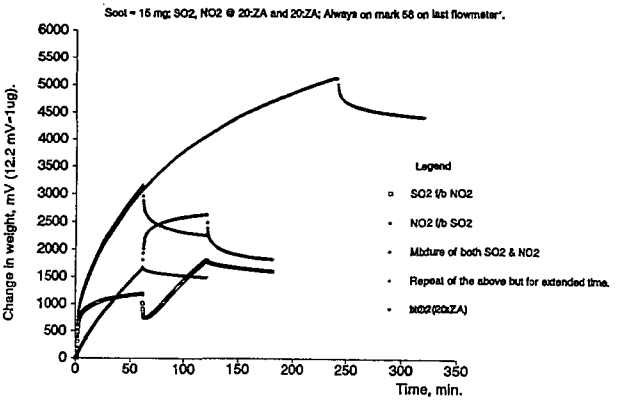

Figure 4. Adsorption of SO2 and NO2 on soot.

Each experiment was carried out with 15 mg soot and 1010 ppm of SO_2 and \ or NO_2 in zero air at 22°C. This sequence of curves reveals the following:

1. the typical SO_2 adsorption curve is interrupted by a flow of NO_2 at 60 min, the SO_2 desorption (as P_{SO2} --> 0) followed within 4 minutes by the increase in mass accompanying NO_2 chemisorption;
2. the inverse order of flow shows an adsorption of SO_2 following NO_2 of about 16% less than untreated soot; because NO_2 is mostly chemisorbed, the SO_2 flow does not result in visible mass loss.;
3. a flow of SO_2 and NO_2 together yields an increase in mass 11% higher than separately; this curve is reproduced over the longer term, with the loss of mass (mostly SO_2) about the same in each case when the same zero air purge is used;
4. small amounts of NO_2 are lost through zero air purge, indicating a small amount (9.7%) of NO_2 is loosely bound (physisorbed) under these conditions.

EPR measurements of spin density, the principles of which are discussed in our first symposium paper (8), have been carried out on this system as well, and the results are summarized in Figure 5. The decrease in corrected normalized integral (CNI) of soot's EPR signal with the pressure of paramagnetic NO_2 is evident as is the lack of effect of diamagnetic SO_2. When experiments in which SO_2 adsorption is followed by NO_2 adsorption and vice-versa are carried out, there clearly is no effect of the presence of SO_2 on the interaction of NO_2 with the unpaired electrons of soot. These data are consistent with the displacement of some adsorbed SO_2 by NO_2, however, as indicated by the microgravimetric data of Figure 4. This does not account for any presence of O_2 in zero air and its occupation of free radical sites, which would be reflected microgravimetrically in changes in capacity for SO_2 under some conditions.

Separate experiments have ehown that soot treated with 140 torr NO_2, resulting in a reduction of CNI from 1.62×10^7 to 0.61×10^7, undergoes an increase of 10% in unpaired spins upon exposure to air. Evacuation at 10^{-4} torr further increases the CNI to 1.05×10^7 while the addition of air returns it to 0.67×10^7, the cycle continuing to change the spin density of carbon in this manner. It appears that O_2 does compete effectively with the small physisorbed fraction (~10%) of adsorbed NO_2 for

unpaired electron sites.

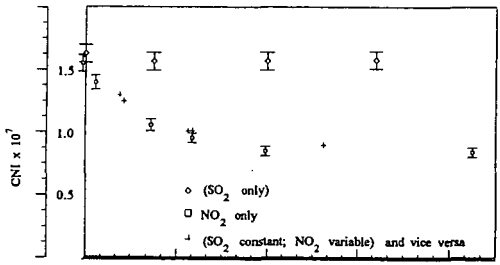

Figure 5. CNI against gas pressure

NO Adsorption

The FT-IR evidence presented for the lack of NO reactivity with soot at ambient temperatures (3) is supported by EPR studies of NO and NO + O_2 adsorption. Figure 6 shows the effects of O_2 and

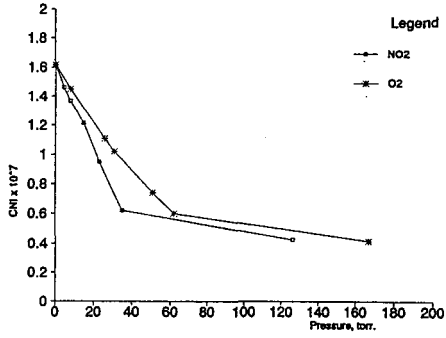

Figure 6. Effects of oxidants on the normalized integral of soot.

NO adsorption on the CNI of soot beyond a linear range below 50 torr to pressures of nearly 170 torr. The similar but slightly lesser effect of NO on spin density, as compared with that of O_2, forms the basis for the experiments summarized in Figure 7. Exposure of the soot to air following adsorption of NO at 8 and 62 torr shows the effect on CNI expected below and at / or above surface saturation by NO, respectively. The surprising effect is the more complete removal of paramagnetic species NO + O_2 to yield a higher CNI than the initial. This consistent result shows NO-assisted removal of that O_2 still remaining on the soot surface following the initial evacuation and mild thermal treatment. It is to be contrasted with the similar experiment with NO_2 described above. NO apparently is reversibly adsorbed and, probably through formation of a complex (or reaction) with pore O_2, even raises the spin density of the soot though its evacuation.

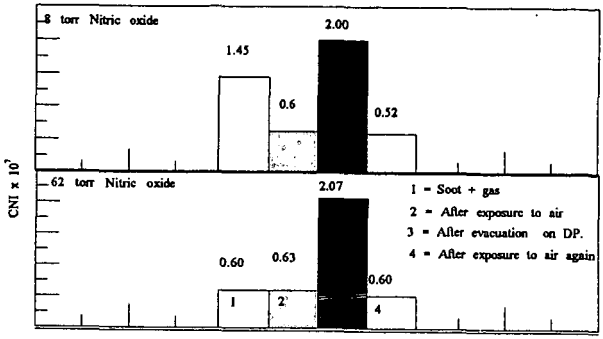

Figure 7 . Plot of CNI for Soot/gas-Air exposure-Evacuation-Exposure to air sequence .

ACKNOWLEDGEMENTS

The authors gratefully acknowledge the support of the National Science Foundation for this research through grant ATM-9200923. Gratitude also is expressed to S. S. and G. R. Eaton of the Department of Chemistry for assistance with, and for the use of, the EPR instrumentation.

REFERENCES

1. Akhter, M. S.; Chughtai, A. R. ; Smith, D. M., J. Phys. Chem., 1984, 88, 5334.
2. Chughtai, A. R. ; Gordon, S. A.; Smith, D. M., Carbon 1994, 32,405.
3. Smith D. M.; Welch, W. F.; Graham, S. M.; Chughtai, A. R.; Wicke, B. G.; Grady, K. A., Appl. Spectrosc. 1988, 42,674.
4. Chughtai, A. R.; Welch, W. F.; Akhter, M. S.; Smith, D. M., Appl. Spectrosc. 1990, 44, 294.
5. Chughtai, A. R.; Welch, W. F.; Smith, D. M., Carbon 1990, 28, 411.
6. Smith D. M.; Keifer, J. R.; Novicky, M.; Chughtai, A. R., Appl. Spectrosc. 1989, 43, 103.
7. Chughtai, A. R.; Brooks, M. E.; Smith, D. M., J. Geophys. Res., 1995, in press.
8. Smith D. M.; Atteya, M. M. O; Konowalchuk, B. K.; Rosenberger, M. L.; and Chughtai, A. R., *Symposia Preprints, Div. Fuel Chemistry, Am. Chem. Soc.*, New Orleans, 1996.
9. Billinge, B. H. M., in *Second Conference on Industrial Carbon and Graphite*, Society of Chemical Industry, London, 1966; p. 399.
10. Hayward, D. O.,; Trapnell, B. M. W., *Chemisorption*, 2nd ed., Butterworths, London, 1964, p. 167.
11. Davini, P., Carbon, 1994, 32, 349.

TPD STUDY ON SO_2 GASIFICATION OF COAL CHAR

T. Takarada and Y. Suzuki
Faculty of Engineering, Gunma University
1-5-1 Tenjin-cho, Kiryu, Gunma, Japan 376

Keywords; coal char, SO_2 gasification, temperature-programed desorption

INTRODUCTION

Elementary sulfur can be recovered from SO_2-containing gas by a gasification reaction between carbon and SO_2. Limited studies on the reaction of coal with SO_2 have been reported[1), 2)]. Works on the mechanism of gasification of coal chars with oxygen-containing gases such as O_2, H_2O, CO_2 have been carried out for a long time. Recently, many temperature-programed desorption (TPD) studies on the surface complexes formed by the chemisorption of oxygen-containing gases on carbon have been performed, because the technique is very useful to evaluate the surface active sites in detail. We already investigated the effects of coal type, mineral matter and catalyst addition on the SO_2 gasification rate of coal chars[3)]. In this study, nine coal chars derived from coals ranging from brown coal to anthracite, three demineralized coal chars and catalyst-loaded coal chars were chemisorbed with SO_2. TPD patterns of samples were obtained and the relationship between the reactivities of chars and the TPD patterns was discussed. The comparison of TPD pattern of SO_2-chemisorbed char with that of O_2-chemisorbed char was also performed.

EXPERIMENTAL

Sample

Nine coals were used in this study. Carbon contents of nine coals are as follows; Loy Yang (LY) 65.1, Yallourn (YL) 66.1, Morwell (MW) 67.9, Sufco (SF) 73.9, Taiheiyo (TH) 77.0, Leopold (LP) 79.9, Liddell (LD) 83.5, Smokyriver (SR) 90.6, Kuznetsky (KN) 90.7 (wt%, daf). The analyses of these coals have been described elsewhere[3)]. The particle size of coal was 32-60 mesh. To examine the effect of the inherent mineral matter on the reactivity and TPD pattern of char, YL, MW and TH coals were treated with a dilute HCl solution for 2 h.

Method of catalyst addition

Yallourn coal, Australian brown coal, was used for catalytic gasification experiments. Potassium carbonate, sodium hydroxide, calcium hydroxide, magnesium hydroxide and iron nitrate were used as the starting materials for catalyst impregnation. Yallourn coal treated with a dilute HCl solution was impregnated with an aqueous solution of catalyst salt and dried at 107°C. The metal to coal ratio was ranged from 1:10 to 1:200 by weight.

Reactivity measurement

The gasification reaction was conducted in a thermo-balance (Shinku-Riko, TGD-7000). The temperature was raised to the gasification temperature at a rate of 60 °C/min after evacuation and substitution with nitrogen gas. After a stationary condition was established, SO_2-N_2 gas (SO_2 concentration:5.2vol%) was introduced and the gasification of char was initiated. The isothermal reaction was allowed to continue for 2 - 10 h.

TPD experiment

TPD experiments were carried out in a fixed bed reactor with gas analysis systems. About 100mg of coal sample was placed in the fixed bed reactor and heated up to 950°C at a heating rate of 60°C/min with flowing Ar gas. The devolatilization of sample was allowed to continue for 30min. Then, two kinds of chemisorption procedures were performed as follows. Procedure 1: samples were cooled down to 150°C and then exposed to either SO_2 (5.2vol%) or O_2 (20vol%) for 60min. Procedure 2: the sample was cooled down to 800°C. Then, SO_2 gas was introduced in the reactor and the sample was cooled down to 500°C at a cooling rate of 60°C/min with flowing SO_2/Ar gas. During the adsorption stage, a part of char (less than 10% of conversion) was gasified. After evacuation and substitution with Ar gas, the samples were heated up to 900°C

or 950°C at a heating rate of 5°C/min or 10°C/min under Ar flow. The gases desorbed during the heat-treatment were continuously analysed with quadrupole mass spectrometer (Nichiden Anelva AQA-200) and the total amounts of CO and CO_2 gases evolved were analysed with a gas chromatography and IR gas analysers.

RESULTS AND DISCUSSION

TPD patterns of SO_2- and O_2-chemisorbed MW chars

The TPD patterns of SO_2- and O_2-chemisorbed MW char prepared by procedure 1 are shown in Figures 1 and 2. The TPD pattern strongly depended on the type of adsorbed gas. A broad desorption of CO_2 for O_2-chemisorbed char was obtained in the range from 150°C to 650°C as previously reported by Zhang et al.[4]. On the other hand, a sharp desorption peak of CO_2 for SO_2-sorbed char appeared at around 700°C. Relatively broad desorption of CO for O_2-sorbed char was observed, while CO gas was evolved at higher temperature range for SO_2-sorbed char. It is noteworthy that no desorptions of both CO_2 and CO for SO_2-sorbed char were detected at a low temperature range below 450°C.

Reactivities and TPD patterns of raw coal chars

Figure 3 shows TG curves obtained for nine coal chars. The sample weight gradually increased in the earlier gasification stage, and then decreased. The increase in weight may be due to the adsorption of SO_2 gas to char surface and to the reaction between mineral matter in char and SO_2. The weight decrease is due to the SO_2 gasification of coal char. The reactivity and the gasification profile strongly depended on coal type. The reactivities of chars derived from coals with carbon content >80 wt% were small and those of lower-rank coal chars were high and widely spread. These results are quite similar to those obtained in the study on the steam gasification of coal chars[5]. The TPD patterns for nine coal chars prepared by procedure 2 were obtained . Four examples are shown in Figure 4. The TPD pattern depended on the coal type. A large and sharp CO_2 peak at around 700°C for MW char and YL char was observed. TH char gave a small CO_2 peak. Little CO_2 gas desorption for LP char was obtained. The TPD patterns for higher rank coal chars such as KN, SR and LD were quite similar to that of LP char. A broad desorption of CO was observed for all coal chars examined. The correlation between the reactivity and the amount of gases desorbed was examined. It was found that the amount of CO desorbed shows a good correlation with the gasification reactivity.

Effect of mineral matter on reactivity and TPD pattern

The effect of acid treatment on the reactivity and TPD profile was examined. The results are shown in Figures 5 and 6. Extraction of coal samples with HCl solution caused appreciable decrease in gasification rate, almost complete disappearance of CO_2 desorption peak and considerable decrease in CO desorption peak. Ratcliffe et al. have reported that acid treatments of lignite caused a decrease in SO_2 gasification rate of char[1]. It is well known that exchangeable cations such as Na and Ca show high activity for steam gasification of low rank coal chars[5]. The decreases in the rate and the amount of gases desorbed may be due to the removal of catalyst metals in mineral matter.

Effect of catalyst addition on reactivity and TPD pattern

The effect of catalyst addition on the reactivity and TPD pattern was investigated (Figures 7 and 8). The gasification profile and TPD pattern was strongly affected by the catalyst addition. The addition of alkaline metals such as K and Na enormously enhanced not only the gasification rate but also the amount of gases desorbed. Relatively sharp desorption peaks of CO_2 and CO for alkaline metal-loaded chars were observed at around 780°C and 830°C, respectively. Both the reactivity and the amount of gases evolved depended on the potassium loading (Figures 7 and 9). In the case of Ca catalyst, although the CO_2 desorption peak at 700°C was increased, the effectiveness of Ca as catalysts for SO_2 gasification of char was quite small. The results show that all CO_2 evolved are not responsible for the gasification rate. XRD measurements of Ca-loaded char showed that Ca catalyst was gradually transformed to CaS during SO_2 gasification of char. The TPD results obtained in this study give the information of initial reactivity of Ca-loaded char. Further investigations are needed to reveal the relationship among the TPD pattern of Ca-loaded char, the activity and chemical form of Ca catalyst.

CONCLUSIONS

The TPD patterns of coal chars chemisorbed with SO_2 gas were determined. The TPD pattern depended on the coal type, mineral matter and catalyst type. Alkaline metals such as Na and K enormously enhanced the gasification rate and the amount of CO_2 and CO evolved. A relatively good correlation was obtained between the reactivity of char and the amount of CO gas desorbed during TPD.

REFERENCES

1. Ratcliffe, C. T. and Pap, G., FUEL, 59, 244 (1980)
2. Abramowitz, H. et al., Carbon, 14, 84 (1976)
3. Takarada, T. et al., Proceedings of the 7th ICCS, p.170 (1993)
4. Zhang, Z.-G. et al., Energy & Fuels, 2, 679 (1988)
5. Takarada, T. et al., FUEL, 64, 1438 (1985)

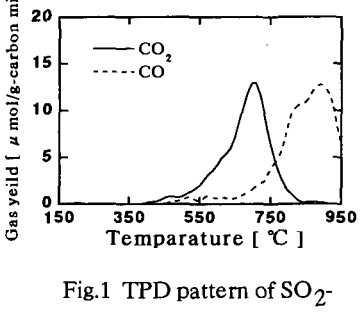

Fig.1 TPD pattern of SO_2-chemisorbed MW char.

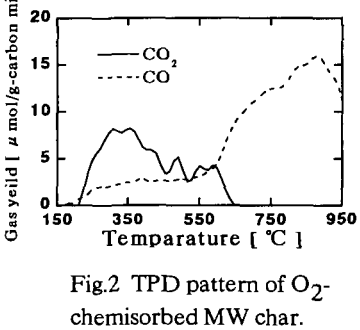

Fig.2 TPD pattern of O_2-chemisorbed MW char.

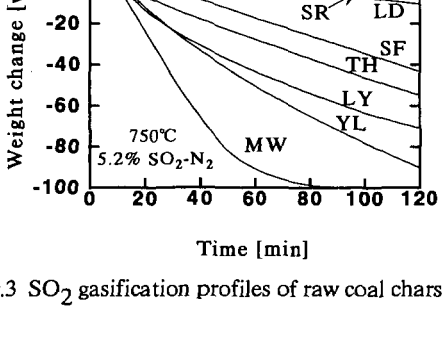

Fig.3 SO_2 gasification profiles of raw coal chars at 750°C.

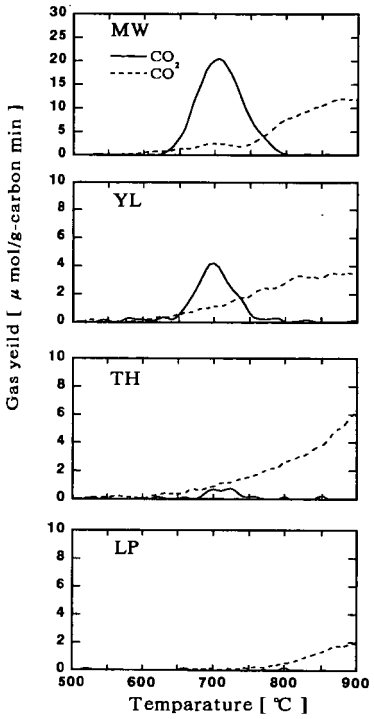

Fig.4 TPD patterns of raw coal chars.

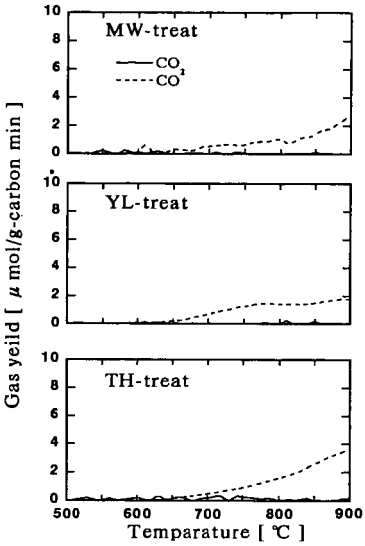

Fig.5 TPD patterns of demineralized coal chars.

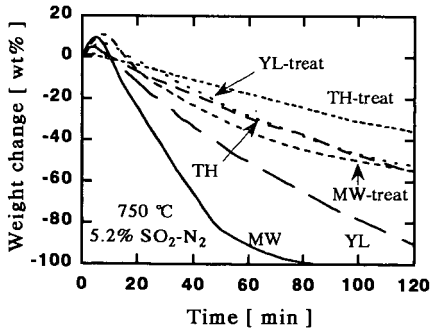

Fig.6 Effect of acid treatment on SO_2 gasification profile at 750℃.

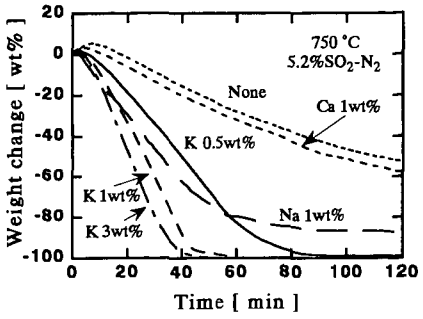

Fig.7 Catalytic SO_2 gasification of YL char at 750℃.

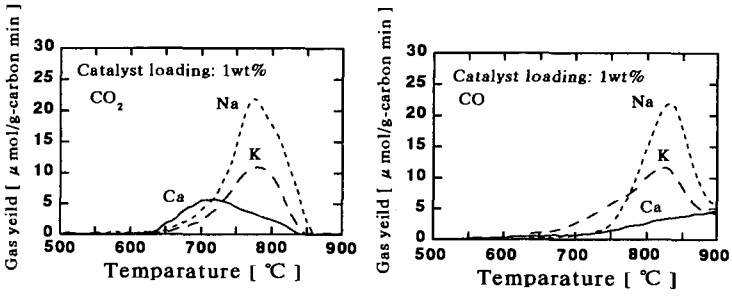

Fig.8 TPD patterns of catalyst-loaded YL chars.

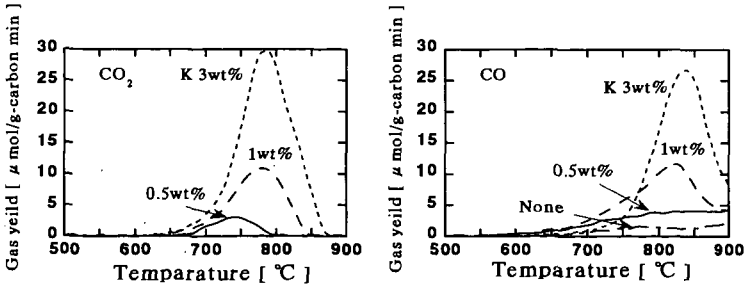

Fig.9 TPD patterns of K-loaded YL chars.

This page left intentionally blank.

THE MECHANISM OF SO_2 REMOVAL BY CARBON

Anthony A. Lizzio[1] and Joseph A. DeBarr[1,2]

[1]Illinois State Geological Survey, 615 East Peabody Drive, Champaign, IL 61820
[2]Environmental Engineering and Science Program, University of Illinois, Urbana, IL 61801

Keywords: activated char, sulfur dioxide, temperature programmed desorption.

INTRODUCTION

There are a number of research groups currently involved in the development of novel carbon-based processes and materials for removal of SO_2 from coal combustion flue gas [1-16]. The type of carbon used more often than not dictates the economic viability of a given process. A high quality carbon adsorbent for SO_2 removal should have a high adsorption capacity, rapid adsorption kinetics, low reactivity with oxygen, minimal loss of activity after regeneration, low pressure drop, high mechanical strength, and low cost. The objective of this study [17-23] has been to produce activated char from Illinois coal with optimal SO_2 removal properties, and to gain a better understanding of SO_2 removal by carbon.

The reaction of SO_2 with carbon in the presence of O_2 and H_2O at relatively low temperatures (80-150°C) involves a series of reactions that leads to the formation of sulfuric acid as the final product. The overall reaction is $SO_2 + 1/2\ O_2 + H_2O + C \text{ ----> } C\text{-}H_2SO_4$. Most studies that have sought to maximize the SO_2 removal capabilities of a carbon only assume a certain mechanism for SO_2 adsorption and conversion to H_2SO_4 is operable. In the literature [1-5,8,10,24], the following reaction sequence has usually been presented before beginning any discussion on SO_2 removal by carbon.

$$C + SO_2 \text{ ----> } C\text{-}SO_2$$
$$C + 1/2\ O_2 \text{ ----> } C\text{-}O$$
$$C + H_2O \text{ ----> } C\text{-}H_2O$$
$$C\text{-}SO_2 + C\text{-}O + C\text{-}H_2O \text{ ----> } C\text{-}H_2SO_4$$

It implies that SO_2, O_2 and H_2O are all adsorbed on the surface of the carbon in close enough proximity and in the proper steric configuration to react and form H_2SO_4. A clearer understanding of this sequence of reactions will no doubt lead to the development of activated carbons better suited for adsorption of SO_2 and its conversion to H_2SO_4. In this paper, we examine the effect of surface area and chemisorbed oxygen on the SO_2 adsorption capabilities of chars prepared from a bituminous coal. Using temperature programmed desorption, we titrate the carbon sites responsible for adsorption of SO_2 and its conversion to H_2SO_4, and based on the experimental results, we propose a more detailed mechanism for SO_2 removal by carbon.

EXPERIMENTAL

Activated chars were prepared from a sample of Illinois Colchester (No. 2) hvC bituminous coal (IBC-102) obtained from the Illinois Basin Coal Sample Program. A 2 in. ID batch, fluidized-bed reactor was used to pyrolyze 200 g of 48x100 mesh coal (N_2, 900°C, 0.5 h) and activate the resultant char (H_2O, 860°C, 30% conversion). The steam activated char was treated with nitric acid (10 M HNO_3, 80°C, 2 h) to modify its pore structure and surface chemistry. The HNO_3-treated char was heated in nitrogen to various temperatures (200-925°C) and held there for 1 h to desorb carbon-oxygen (C-O) complexes formed during the HNO_3 treatment. A commercial activated carbon (Calgon F400) was also studied. SO_2 adsorption capacities of prepared carbons were determined by thermogravimetric analysis using a simulated flue gas containing 2500 ppm SO_2, 5% O_2 and 7% H_2O. Temperature programmed desorption (TPD) experiments (N_2, 25-1000°C, 5°C/min, 1 h at 1000°C) were performed to determine the amount of oxygen adsorbed on the char surface. Further details of the experimental equipment and procedures used in this study are provided elsewhere [19-21].

RESULTS AND DISCUSSION

Table 1 shows how poor the correlation is when SO_2 adsorption capacities of chars are normalized with respect to their surface areas or oxygen contents. It is interesting to note that the steam activated IBC-102 char (H_2O, 860°C) and untreated Calgon F400 carbon have comparable SO_2 adsorption capacities despite a large difference in N_2 BET (77 K) surface area; their CO_2 BET (195 K) surface areas seem to correlate better with SO_2 adsorption capacity. Table 1 also shows that the SO_2 adsorption capacity of the nitric acid treated, thermally desorbed chars increases with increasing thermal desorption temperature. A similar effect of heat treatment (at 800°C) on the SO_2 adsorption capacity of polyacrylonitrile-based activated carbon fibers was recently reported by Mochida and his research group [7,11,12], and attributed to an increase in the number of active sites generated by the evolution of CO and CO_2 during decomposition of C-O functional groups. Davini [25,26] ascribed enhanced SO_2 adsorption on oxidized activated carbon to the presence of basic C-O groups on the carbon surface. Most recently, Kim et al. [13] and Fei et al. [14] proposed that the inherent nitrogen in polyacronitrile and shale oil derived activated carbon fibers, respectively, increases their catalytic activity for SO_2 adsorption and conversion to H_2SO_4.

The TPD profiles of thermally desorbed, nitric acid treated IBC-102 chars shown in Figure 1 indicate

that the absence of oxygen on the carbon surface results in a char with highest SO_2 adsorption capacity (e.g., HNO_3-925°C char). Apparently, carbon atoms, which are not tied up by an adsorbed oxygen atom, have valence electrons that are more available, and are more reactive towards SO_2 adsorption. We, therefore, postulate that the unoccupied or free sites control the uptake of SO_2. It is well known that once carbon is evolved as CO or CO_2 during carbon gasification, a new carbon atom of equal or greater reactivity will be exposed. These newly exposed carbon atoms, coined nascent sites by Phillips et al. [27], in many cases define the surface chemistry of a carbon [28,29]. It is these nascent sites, made active by the thermal desorption treatment at 925°C, that we believe are responsible for enhanced SO_2 adsorption on the HNO_3-925°C char. Nitric acid, being a very strong oxidant, oxidizes the surface of the carbon so that even carbon atoms that would otherwise not react with the oxygen in air are oxidized. Upon thermal desorption treatment, a once relatively unreactive carbon atom is released as CO or CO_2 leaving behind a carbon atom which is then primed to react with SO_2. The evolution of CO or CO_2 also serves to activate the pore structure thereby widening the pores making them more accessible to reactant gases; this could also increase SO_2 adsorption. A parallel study with activated carbon fibers (ACF) in our laboratory [30], however, has shown that ACF with smaller pores (9 Å) and lower surface areas (600 m^2/g) actually adsorb more SO_2 than higher surface area ACF (1900 m^2/g) having larger pores (18 Å). This increase in SO_2 adsorption for low surface area fibers is presumably due to enhanced adsorbent-adsorbate interactions caused by the smaller average pore size [31].

To test our hypothesis that free sites are primarily responsible for SO_2 adsorption, the TPD profiles of the nitric acid treated, thermally desorbed IBC-102 chars of Figure 1 were utilized. We defined the free sites for this series of chars as being those sites that were once occupied by oxygen because of nitric acid treatment, but now, because of the thermal desorption treatment, had become unoccupied or free. To quantify the CO free sites for a given char, say, the HNO_3-725°C char, we subtracted its CO evolution profile from the one of the original nitric acid treated char (Figure 2). The unshaded region in Figure 2 represents the number of free sites that are created by CO evolution during the thermal desorption treatment at 725°C. Table 2 lists the number of both the CO and CO_2 free sites calculated for each of the nitric acid thermally desorbed IBC-102 chars. The last two columns show the SO_2 adsorption capacities normalized with respect to the CO and CO_2 free sites. The SO_2 adsorption capacity is seen to vary by a factor of 1.6 and 2.8 when normalized with respect to CO and CO_2 free sites, respectively. This is an excellent correlation compared to those we found for surface area or adsorbed oxygen (Table 1). To the best of our knowledge, this type of quantitative approach has never before been used to explain SO_2 removal by carbon. The concept of free or unoccupied sites was first postulated and utilized by Laine et al. [32] to explain the gasification reactivity of carbon in oxygen. Our new approach for analyzing TPD data shows that it may be possible to titrate directly the free sites responsible for SO_2 adsorption and conversion to H_2SO_4. A slight variation in this same approach could be used to explain results in other studies that have examined SO_2 removal by carbon. For example, Davini [25,26] found that the SO_2 adsorption capacity of a commercial grade carbon increased with an increase in activation temperature. The activation conditions he used ranged from 300°C in air to 800°C in 2% O_2. Char gasification reactivity studies have shown that less oxygen will adsorb on the carbon surface at higher temperatures and in lower pressures of an oxidizing gas [28,33,34]. The higher temperature used by Davini during activation is likely to have deposited less oxygen on the carbon surface, thus preserving more free sites for reaction with SO_2. In fact, further analysis of his SO_2 and O_2 adsorption data [26] using our concept of free sites shows that the SO_2 adsorption capacities of two groups of carbons that each varied by more than a factor of three, could be made to vary by less than a factor of 1.2 when normalized to the total number of free sites.

This procednre for assessing free adsorption sites was also applied to the Calgon F400 carbon (also a steam activated bituminous coal char). Table 2 shows that there was no significant improvement in the SO_2 capacity of this carbon with our nitric acid, thermal desorption treatment, perhaps because its pore structure was already optimized for adsorption of contaminants. Table 2 shows that the SO_2 adsorption capacity of the Calgon F400 carbons normalized with respect to the number of CO and CO_2 free sites also varies by less than a factor of 2 and 3, respectively. It is interesting to note the almost one to one ratio of SO_2 adsorption capacity to CO free sites for both the IBC-102 and Calgon F400 carbons.

Based on these experimental results, we propose the following sequence of reactions to explain the mechanism of SO_2 removal by carbon.

O_2 Chemisorption	$O_2 + 2\,C \longrightarrow 2\,C\text{-}O$
SO_2 Adsorption	$SO_2 + C \longrightarrow C\text{-}SO_2$
SO_2 Oxidation	$C\text{-}SO_2 + O_2 + C \longrightarrow C\text{-}SO_3 + C\text{-}O$
SO_2 Oxidation	$C\text{-}SO_2 + C\text{-}O \longrightarrow C\text{-}SO_3 + C$
SO_2 Oxidation	$SO_2 + C\text{-}O \longrightarrow C\text{-}SO_3$
H_2SO_4 Formation	$C\text{-}SO_3 + H_2O \longrightarrow C\text{-}H_2SO_4$
Regeneration	$C\text{-}H_2SO_4 \longrightarrow H_2SO_4 + C$

Adsorption of SO_2 and O_2 occurs in parallel on the free carbon active sites (denoted by C). Molecular oxygen dissociates on two free sites to form a pair of C-O complexes. SO_2 competes with O_2 for free sites. The reaction of oxygen with carbon produces a stable C-O complex, which apparently inhibits

SO_2 adsorption. The next step is the oxidation of SO_2 to SO_3. Conceivably, three reactions are possible. The C-SO_2 complex can react directly with molecular oxygen in the vicinity of a free site to form a C-SO_3 intermediate and stable C-O complex. SO_2 oxidation could also be accomplished by the reaction of either the C-SO_2 complex or SO_2 with the C-O complex. However, the occurrence of these two reactions is less likely since we observed an inverse correlation between SO_2 adsorption and stable C-O complex. The conversion of stable C-O complex into a reactive C(O) intermediate, as proposed in recent carbon gasification studies [33-36], may also influence SO_2 adsorption and conversion to H_2SO_4 [19].

According to the SO_2 removal mechanism often presented in the literature (see Introduction), one could assume that the more oxygen adsorbed on the carbon surface, the more SO_2 will be adsorbed. In this study, we have seen that the formation of stable C-O complex during char preparation serves only to occupy otherwise reactive free adsorption sites, and that the C-O complex probably is not an essential reaction intermediate in the conversion of SO_2 to H_2SO_4. It may also be that our TPD method did not titrate those C-O complexes responsible for catalytic oxidation of SO_2 to SO_3, and that a fleeting C(O) complex, formed contemporaneously with SO_2 adsorption and/or by transformation of stable complex into reactive intermediate, acts as the "catalyst." Isotope labelling studies could be useful in determining if such an intermediate exists [37]. Another question is whether SO_2 removal would occur if there was no oxygen in the flue gas and/or adsorbed on the carbon surface. This was resolved by using two of the IBC-102 chars, one with some adsorbed oxygen (HNO_3-525°C) and one with essentially no adsorbed oxygen (HNO_3-925°C). Figure 3 shows that, with 5% O_2 in the flue gas, the HNO_3-925°C char adsorbs the most SO_2. With no oxygen in the flue gas, this char still adsorbs SO_2, but in this case, it is not converting C-SO_2 to H_2SO_4 due to a lack of oxygen. SO_2 adsorption is enhanced for both chars when oxygen is present in the flue gas (compare 0 and 5% O_2 plots in Figure 3). The adsorption of SO_2 on a free site is seen to account for nearly 50% of the weight gain for both chars. This data seems to support the first SO_2 oxidation mechanism, i.e., the one involving the reaction of adsorbed SO_2 with O_2 and a free site to form C-SO_3.

Hartman and Conghlin [38] found the catalytic oxidation of SO_2 to SO_3 by carbon to be the rate determining step in the overall reaction. If the rate determining step is, indeed, catalytic oxidation of SO_2 to SO_3, and assuming that the first SO_2 oxidation reaction is operable, the overall rate of reaction could be expressed as

$$\text{rate} = k_2 [C] [C\text{-}SO_2] [O_2]$$

where k_2 is a fundamental rate constant. The unknowns in this expression are k_2 and the concentration of C-SO_2 complex. At steady state, the rates of each of the reactions in the mechanism presented above are equal to that of the rate determining step, and by definition, the concentration of each of the intermediate species does not change with time. Thus,

$$\frac{d[C\text{-}SO_2]}{dt} = 0 = k_1 [C] [SO_2] - k_2 [C] [C\text{-}SO_2] [O_2]$$

Solving for [C-SO_2],

$$[C\text{-}SO_2] = \frac{k_1 [C] [SO_2]}{k_2 [C] [O_2]} = \frac{k_1 [SO_2]}{k_2 [O_2]}$$

and substituting this into the rate expression,

$$\text{rate} = k_1 [C] [SO_2]^n$$

where n is the order of reaction with respect to SO_2. The rate is then only a function of the concentration of free sites and the partial pressure of SO_2, a departure from the more elaborate rate expressions recently proposed by others (see, for example, refs. [2] and [24]). For concentrations of SO_2 less than 1500 ppm, we found values of n between 0.5 and 1, and for concentrations of SO_2 greater than 1500 ppm, the value of n approached zero (Figure 4). Nevertheless, at a constant partial pressure of SO_2, the rate of SO_2 adsorption and conversion to H_2SO_4 should be directly proportional to the number of free adsorption sites as confirmed by our TPD experiments. It remains to be determined whether this TPD method can be applied to adsorption of other contaminants in flue gas. If so, it could facilitate preparation of activated char optimized for removal of SO_2 as well as other air toxics (e.g., nitrogen oxides, mercury) from combustion flue gas. Recent studies suggest that adsorption of NO_x and reduction to N_2 is more or less controlled by free sites on the carbon surface [39-41].

In the above mechanism, the C-SO_3 intermediate reacts with water to form sulfuric acid. The free site returns to its original state after regeneration. The water adsorbed in the pores may act as a regeneration medium. The acid adsorbed on the carbon surface will be continuously removed by a reservoir of water adsorbed in the pores. As the acid goes into solution, the free site once again becomes reactive towards SO_2 adsorption. Thus, the site can undergo numerous cycles of adsorption/desorption without any external means of regeneration. The production of H_2SO_4 proceeds indefinitely until water adsorbed in the pores becomes saturated with H_2SO_4 and/or the free sites

become occupied with oxygen, at which point the spent carbon needs to be regenerated, e.g., thermal treatment or flushing with water or dilute acid. (The latter treatment will not remove any of the C-O complex). Thus, it can be expected that the amount of water retained in the pore volume of the carbon should determine its equilibrium SO_2 adsorption capacity, which may require more than 40 h to attain (Figure 4); whereas, the rate (or kinetics) of SO_2 adsorption, say, in the first 6 h of adsorption, will be controlled by the number of free sites. In an earlier paper, Jungten and Kuhl [3] hypothesized that the active sites would control the rate of SO_2 adsorption, but this was never verified experimentally. The observed increase in the SO_2 adsorption capacity of nitric acid treated chars with increasing thermal desorption temperature is probably due to both an increase in the concentration of free active sites and in the accessible pore volume of the char. The latter leads to a greater reservoir for storage of dissolved H_2SO_4 and an increased ability to regenerate the active sites for additional SO_2 adsorption.

CONCLUSIONS

In this study, we found the SO_2 adsorption capacity of a coal char to be inversely proportional to the amount of oxygen adsorbed on its surface. Temperature programmed desorption was used to titrate those sites responsible for adsorption of SO_2 and conversion to H_2SO_4. Based on these results, a detailed mechanism for SO_2 removal by carbon was proposed. The derived rate expression shows SO_2 adsorption to be dependent only on a fundamental rate constant and concentration of carbon atoms we designate as free sites. The results obtained here are analogous to those of a recent study [33] which fonnd that a similar relationship exists between the specific rate (R_{sp}) of carbon gasification in carbon dioxide and the number of reactive sites measured initially by transient kinetics (TK) experiments and later confirmed by TPD, i.e., $R_{sp} = k\,[C]$. In that study, TK and TPD were used to titrate those occupied sites or C(O) intermediates responsible for controlling the rate determining desorption step in CO_2 gasification of carbon. The results of both studies seem to support a unified approach to the reactions between carbon and oxygen-containing gases, as most recently proposed by Chen [42] and Moulijn and Kapteijn [43].

ACKNOWLEDGEMENTS

This work was supported by the Illinois Clean Coal Institute through the Illinois Coal Development Board and the United States Department of Energy. The authors gratefully acknowledge the technical assistance of Ms. Gwen Donnals.

REFERENCES

1. Richter, E., Knoblauch, K. and Jungten, H., Proc. 1st Int. Conf. on Processing and Utilization of High Sulfur Coals, 1985, p. 563.
2. Richter, E., Knoblauch, K. and Jungten, H., Gas Separation and Purification 1, 35 (1987).
3. Jungten, H. and Kuhl, H., Chem. Phys. Carbon 22, 145 (1989).
4. Richter, E., Catalysis Today 7, 93 (1990).
5. Tsuji, K. and Shiraishi, I., Proc. Electric Power Research Institute SO_2 Control Symposium, Washington, D.C., 1991, p. 307.
6. Lu, G.Q. and Do, D.D., Carbon 29, 207 (1991).
7. Mochida, I., Hirayama, T., Kisamori, S., Kawano, S. and Fujitsu, H., Langmuir 8, 2290 (1992).
8. Gangwal, S.K., Howe, G.B, McMichael, W.J. and Spivey, J.J., Final Report to U.S. DOE (1993).
9. Gangwal, S.K., Howe, G.B., Spivey, J.J., Silveston, P.L., Hudgins, R.R. and Metzinger, J.G., Envir. Prog. 12, 128 (1993).
10. Lu, G.Q. and Do, D.D., Gas Separation and Purification 8, 17 (1994).
11. Kisamori, S., Mochida, I. and Fujitsu, H., Langmuir 10, 1241 (1994).
12. Kisamori, S., Kurado, K., Kawano, S., Mochida, I., Matsumura, Y. and Yoshikawa, M., Energy and Fuels 8, 1337 (1994).
13. Kim, J.-Y., Hong, I. and Lee, J.G., Proc. 22nd Biennial Conf. on Carbon, San Diego, CA, 1995, p. 534.
14. Fei, Y., Sun, Y.N., Givens, E. and Derbyshire, F., ACS Preprints, Div. Fuel Chem. 40 (4), 1051 (1995).
15. Vladea, R.V., Hinrichs, N., Hudgins, R.R., Suppiah, S. and Silvestou, P.L., ACS Preprints, Div. Fuel Chem., New Orleans, LA, 1996 (in press).
16. Mochida, I., Kuroda, K., Yasutake, A., Yoshikawa, M., Matsumura, Y., ACS Preprints, Div. Fuel Chem., New Orleans, LA, 1996 (in press).
17. Lizzio, A.A., DeBarr, J.A., Kruse, C.W., M., Donnals, G.L. and Rood, M.J., "Production and Use of Activated Char for Combined SO_2/NO, Removal," Final Technical Reports to the Illinois Clean Coal Institute (1994, 1995).
18. DeBarr, J.A. and Lizzio, A.A., Proc. Int. Conf. on Carbon, Granada, Spain, 1994, p. 268.
19. Lizzio, A.A. and DeBarr, J.A., Fuel 1995 (in press).
20. DeBarr, J.A., "The Role of Free Sites in the Removal of SO_2 from Simulated Flue Gases by Activated Char," M.S. Thesis, University of Illinois at Urbana-Champaign (1995).
21. DeBarr, J.A., Lizzio, A.A. and Rood, M.J., Proc. 88th Annual Air and Waste Management Assoc. Meeting, San Antonio, TX (1995).
22. DeBarr, J.A. and Lizzio, A.A., Proc. 22nd Biennial Conf. on Carbon, San Diego, CA, 1995, p. 562.
23. Lizzio, A.A. and DeBarr, J.A., Proc. 12th Int. Annual Pittsburgh Coal Conf., Pittsburgh, PA, 1995, p. 652.
24. Gall, E. and Kast, W., Chem. Eng. Sci. 45, 403 (1990).
25. Davini, P., Fuel 68, 145 (1989).
26. Davini, P., Carbon 28, 565 (1990).
27. Phillips, R., Vastola, F.J. and Walker, P.L., Jr., Carbon 8, 197 (1970).
28. Boehm, H.P. and Bewer, G., Proc. 4th London Int. Conf. on Carbon and Graphite, 1974, p. 344.
29. Leon y Leon, C.A. and Radovic, L.R., Chem. Phys. Carbon 24, 213 (1994).
30. DeBarr, J.A., Lizzio, A.A. and Daley, M.A., ACS Preprints, Div. Fuel Chem., New Orleans, LA, 1996 (in press).
31. Foster, K.L., Fuerman, R.G., Economy, J., Larson, S.M. and Rood, M.J., Chem. Mater. 4, 1068 (1992).
32. Laine, N.R., Vastola, F.J. and Walker, P.L., Jr., Phys. Chem. 67, 2030 (1963).
33. Lizzio, A.A., Jiang, H. and Radovic, L.R., Carbon 28, 7 (1990).
34. Radovic, L.R., Jiang, H. and Lizzio, A.A., Energy and Fuels 5, 68 (1991).
35. Back, M.H., Carbon 29, 1290 (1991).
36. Radovic, L.R., Karra, M. and Skokova, K., Proc. 22nd Biennial Conf. on Carbon, San Diego, CA, 1995, p. 636.
37. Kapteijn, F., Meijer, R. and Moulijn, J.A., Energy and Fuels 6, 494 (1992).
38. Hartman, M. and Coughlin, R.W., Chem. Eng. Sci. 27, 867 (1972).
39. Teng, H., Snuberg, E.M. and Calo, J.M., Energy and Fuels 6, 398 (1992).
40. Yamashita, H., Tomita, A., Yamada, H., Kyotani, T. and Radovic, L.R., Energy and Fuels 7, 85 (1993).
41. Mochida, I., Kisamori, S., Hironaka, M., Kawano, S., Matsumura, Y. and Yoshikawa, M., Energy and Fuels 8, 1341 (1994).
42. Chen, S.G., Yang, R.T., Kapteijn, F. and Moulijn, J.A., Ind. Eng. Chem. Res. 32, 2835 (1993).
43. Moulijn, J.A. and Kapteijn, F., Carbon 33, 1155 (1995).

Table 1. Correlation of SO_2 adsorption capacity with surface area and adsorbed oxygen.

Sample	SO_2 Capacity[1] (mg SO_2/g char)	N_2 BET (m^2/g)	CO_2 BET (m^2/g)	SO_2/N_2 (mg/m^2)	SO_2/CO_2 (mg/m^2)	O_2 (wt%)	SO_2/O_2
IBC-102, 900°C, 0.5 h	7	1.2	98	5.8	0.07	0.5	1.40
IBC-102, 900°C; H_2O, 860°C	176	220	613	0.80	0.29	1.1	16.0
IBC-102, 900°C; H_2O, 860°C; HNO_3	---[3]	400	585	0.06	0.04	16.4	---[3]
IBC-102, 900°C; H_2O, 860°C; HNO_3, 525°C	91	460	693	0.20	0.13	5.9	1.54
IBC-102, 900°C; H_2O, 860°C; HNO_3, 725°C	241	500	727	0.48	0.33	1.6	15.0
IBC-102, 900°C; H_2O, 860°C; HNO_3, 925°C	287	550	726	0.05	0.39	0.5	57.4
Calgon F400	206	1000	1000	0.21	0.21	0.5	41.2
Calgon F400, HNO_3	---[3]	---[3]	---[3]	---[3]	---[3]	15.7	---[3]
Calgon F400, HNO_3, 200°C	46	600	---[3]	0.08	---[3]	14.3	0.32
Calgon F400, HNO_3, 525°C	117	456	---[3]	0.26	---[3]	5.6	2.09
Calgon F400, HNO_3, 725°C	156	533	---[3]	0.29	---[3]	3.4	4.59
Calgon F400, HNO_3, 925°C	214	463	---[3]	0.46	---[3]	1.7	12.6

[1] SO_2 capacity determined after 6 h.
[2] not determined.

Table 2. Correlation of SO_2 adsorption capacity with free adsorption sites.

Sample	SO_2 capacity[1]	Adsorbed oxygen[1]	CO/CO_2	CO free sites[1,2]	CO_2 free sites[1,2]	SO_2 capacity (CO free sites)	SO_2 capacity (CO_2 free sites)
IBC-102, HNO_3	---[3]	5.12	1.4	0	0	---[3]	---[3]
IBC-102, HNO_3, 525°C	0.142	1.84	6.7	1.37	2.59	1.04	0.55
IBC-102, HNO_3, 725°C	0.376	0.50	12.8	3.35	2.94	1.12	1.28
IBC-102, HNO_3, 925°C	0.448	0.16	---[4]	3.90	3.01	1.15	1.49
Calgon F400, HNO_3	---[3]	4.91	1.4	0	0	---[3]	---[3]
Calgon F400, HNO_3, 200°C	0.072	4.47	0.8	0.86	0.34	0.84	2.12
Calgon F400, HNO_3, 525°C	0.183	1.75	7.6	1.28	2.52	1.43	0.73
Calgon F400, HNO_3, 725°C	0.244	1.06	5.5	2.26	2.56	1.08	0.95
Calgon F400, HNO_3, 925°C	0.334	0.53	5.4	3.28	2.75	1.02	1.22

[1] moles/kg char.
[2] calculated-assuming that 1 chemisorbed O_2 evolved as 2 CO during TPD is equivalent to 2 CO free sites, and 1 chemisorbed O_2 evolved as 1 CO_2 is equivalent to 1 CO_2 free site.
[3] not determined.
[4] CO_2 concentration below detectable limits.

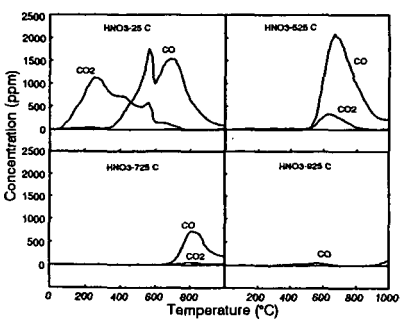

Figure 1. TPD profiles of nitric acid/thermally desorbed IBC-102 chars.

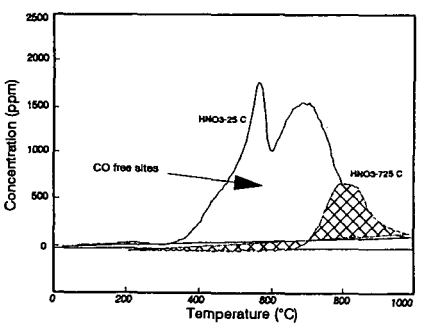

Figure 2. Subtraction of CO evolution profiles to determine CO free sites.

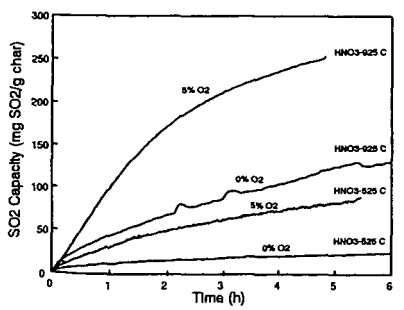

Figure 3. Effect of oxygen on SO2 adsorption.

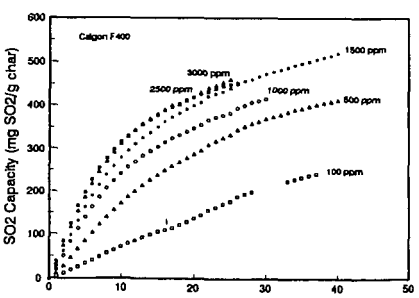

Figure 4. Effect of SO2 concentration.